Revision 2

Graphite paradox in Baikal geyserite paleovalley, Russia

Tatyana G. Shumilova[1]*, Yulia V. Danilova[2], Joachim Mayer[3], Sergey I. Isaenko[1] and Boris S. Danilov[2], Vasily V. Ulyashev[1]

[1] Institute of Geology, FRC Komi SC UB RAS Pervomayskaya st., 54, Syktyvkar, 167982, Russia; shumilova@geo.komisc.ru, ORCID: 0000-0002-1772-3606;

[2] Institute of Earth's Crust, SB RAS Lermontov st., 128, Irkutsk, 664033, Russia; e-mail: jdan@crust.irk.ru, ORCID: 0000-0002-6454-3552;

boris@crust.irk.ru; ORCID: 0000-0002-3262-6636;

[3] Central Facility for Electron Microscopy, RWTH Aachen University Ahornstrasse 55, D52074 Aachen, Germany; e-mail: mayer@gfe.rwth-aachen.de

* Correspondence: tg_shumilova@mail.ru; Tel.: +79212240970

ABSTRACT

Natural graphite, a polygenic mineral, is a product of regional, contact, impact metamorphism, and magmatic or fluid deposition. In fluid-deposited graphite, aqueous C–O–H systems play a special role in determining the characteristics of hydrothermal products by shifting the chemical equilibrium. From this viewpoint, the recently discovered carboniferous mineralization in the Baikal hydrothermalites has attracted increasing interest with regard to graphite crystallization under the influence of low-pressure low-temperature (LPLT) carboniferous H_2O-rich fluids. Herein, we studied graphite mineralization in the geyserites and travertines of the Baikal geyserite paleovalley (Eastern Siberia, Russia) by applying a multitude

of mineralogical studies. Optical, scanning, transmission electron, and atomic force microscopy, energy dispersive spectroscopy, Raman spectroscopy, and carbon isotopic composition analyses of graphite, carbonate carbon, and oxygen in both the hydrothermalites and host rocks were conducted. The obtained results revealed a number of peculiar features regarding the graphite in geyserites and travertines. We found that Baikal graphite, earlier predicted to be a product of hydrothermalites, generally occurs as a relict graphite of the host metamorphic rocks with partial in situ redeposition. The newly formed LPLT fluid-deposited graphite is characterized by micrometer- and submicrometer-sized idiomorphic crystallites overgrown on the relict metamorphic graphite seeds and between calcite sinter zones during the last stage of travertine formation. The results present additional valuable data for understanding the mechanism, range of the formation conditions, and typomorphism of fluid-deposited graphite with probable crystallization from carbon solution in the C–O–H system at LPLT conditions.

Keywords: graphite; geyserite; travertine; hydrothermal conditions; C–O–H fluid; fluid deposition; paleovalley; Baikal rift zone

INTRODUCTION

Natural graphite is formed either from organic matter during metamorphic processes (regional, contact, and impact metamorphism) or from fluid mineralization resulting from carbon containing fluids (Beyssac et al., 2002, 2003; Luque et a., 2011; Jaszczak et al., 2003, 2007; Pasteris and Wopenka, 1991; Shumilova et al., 2003; Shumilova et al., 2018; Wopenka

and Pasteris, 1993 and others). Metamorphic graphite is characterized by a wide range of crystallinity levels (from poorly crystalline to high ordered crystalline structures) resulting from a multitude of metamorphic grades, and can be used for thermodynamic calculations (Beyssac et al., 2002, 2003; Wopenka and Pasteris, 1993). Fluid-deposited graphite, regardless of its formation conditions, differs from the metamorphic graphite by a universal high crystalline structure and has different well-shaped crystalline habits (Luque et al., 1998; Luque et al., 2009a; Luque and Rodas, 1999; Jaszczak et al., 2003, 2007; Pasteris, 1999), in contrast to the preferable colloform, cryptocrystalline, and flaky graphite crystals found in metamorphic rocks. Some studies have stated that metamorphic and fluid-deposited varieties can occur simultaneously in the same geological object, and sometimes, fluid-deposited graphite can overgrow the earlier formed metamorphic graphite (Luque et al, 2011). The nature of a certain graphite variety can be identified via isotopic studies, which utilize a series of geological data to recognize the different carbon sources of magmatic and sedimentary carbonates, organic matter assimilation, and devolatilization origin and mixture of different graphite carbon sources (Luque et al., 2011). Fluid-deposited graphite is a result of carbon bearing CO_2, $CO_2 + CH_4$, CO_2–CH_4–H_2O, and CH_4 fluids, where H_2O plays an important role in both graphite initial deposition and precipitation (Duke and Rumble, 1986). Open C–O–H systems with H_2O-rich fluid are of increasing interest for understanding fluid-deposited graphite formation. Thus, the graphite occurrences in the Late Quaternary hydrothermalites formed from the aqueous fluid (travertines and geyserites) of the

Baikal rift zone (Danilova et al. 2016; Shumilova et al. 2009, 2011; Sklyarov et al, 2014) are of special interest.

Hydrothermal sources are also the subjects of intensive research and use (Altunel and Hancock 1993; Pentecost and Viles 1994; Pentecost 1995; Minissale et al. 2002; Jones and Renaut 2003; Lund et al. 2005; Omelon et al. 2006; Renaut et al. 2008; Crossey et al. 2009; Gibert et al. 2009; Shumilova et al. 2018 and others). As these sources are widespread, several of these are a part of active tourism and health resorts; examples include: Pamukkale in Turkey (Dilsiz et al. 2004; Pentecost 2005), Italy hot springs (Cascate del Mulino, Saturina, terme di San Filippo et al.), the Kamchatka valley (Naboko et al. 1999), the Mammoth Hot Springs at Yellowstone in the USA (Fouke 2000), and the Iceland hot springs (Fraedrich and Heidari 2019). Furthermore, hot springs are useful as hydrothermal energy sources. In some cases, hot springs form large travertine deposits that are used as construction and ornamental materials (Dilsiz et al. 2004; Lund et al. 2005). The other type of the hot springs deposits are geyserites which have been studied intensively with respect to active volcanism and post volcanic hydrothermal activity as well as in connection with the vital activities of organisms under extreme conditions and microfossils; evidence of the first manifestations of life on land has been discovered in hot spring deposits (Tatarinov et al. 2006; Van Kranendonk 2006; Harris et al. 2009; Campbell et al. 2015; Djokic et al. 2017; Zhegallo et al. 2018).

The formation of the majority of the current surface hydrotherms is associated with relatively low temperatures, approximately 20–70 °C. Under these conditions thermal waters among carbonate sediments precipitate travertine deposits. However, there are instances of

travertine formation at slightly higher temperatures, reaching 97.5 °C (Renaut et al. 2013). Siliceous geyserites form at moderately high temperatures, generally up to 100 °C.

From this viewpoint, the Late Quaternary graphite geyserites and travertines of the Ol`khon area and northern tip of Ol`khon Island on Lake Baikal (Eastern Siberia, Russia) are unique geological and petrological objects, as detailed by Sklyarov et al. (2014), as their formation proceeded at a minimum temperature of 400 °C. Conclusions regarding the high-temperature formation of these geyserites are mainly based on carbon phases, such as newly formed graphite and carbyne (Shumilova et al. 2009, 2011), which are shown to form with the participation of carbonaceous fluid (Danilova et al. 2016).

However, a detailed study on the typomorphic features of graphite in geyserites and travertines of the Baikal Paleovalley indicated a more complex developmental history, which is based on metamorphic graphite dissolution and in situ redeposition. Note that despite the known graphite occurrences deposited from C–O–H fluids, objects that coexist with free H_2O and graphite in low-pressure low-temperature (LPLT) hydrothermalites have not been found elsewhere. Therefore, these findings involve unique objects of mineralogical and geological significance.

MATERIALS AND METHODS

Samples for this study were provided by E.V. Sklyarov. The travertine and geyserite samples were from the natural outcrops described in Sklyarov et al. (2004; 2007; 2014). Herein, we used large square polished sections (up to 5–10 cm in size) and petrographic polished sections. Note that some of the analytical analyses were conducted directly “in situ,” and the graphite concentrates were chemically separated from rocks for use in the bulk structural, isotopic, and micromorphological studies. For detailed isotopic studies, individual particles of

graphite were separated "grain-by-grain" with a needle and processed with dilute hydrochloric acid to remove the host carbonate matrix. Most of the mineralogical analyses were conducted at the CCU Geoscience (IG Komi SC UB RAS, Syktyvkar).

The carbon isotope composition of the graphite was measured using an analytical complex Flash EA instrument connected with a mass spectrometer Delta V Advantage (Thermo Fisher Scientific, Germany). The carbonate decomposition and carbon and oxygen isotopic measurements were conducted using an analytical complex Gas Bensh II with a mass-spectrometer Delta V Advantage. The measurement errors for carbon, $\delta^{13}C$ (PDB), and oxygen, $\delta^{18}O$ (SMOW), for the carbonates were ± 0.01 ‰ and 0.02 ‰ respectively (1σ), for the carbon of graphites ± 0.15 ‰ (1σ) (PDB). These studies were performed at the IG Komi SC UB RAS (Syktyvkar) and UIGGM SB RAS (Novosibirsk). Lab preparations and measurements were used to avoid contamination from any kind of environmental carbon (any carbon source present in the laboratory, e.g., grease from skin), only chemically pure acids and gases were used for preparations and analytical methods.

Scanning electron microscopy (SEM; VEGA 3 TESCAN, Tescan, Czech Republic) and energy dispersive spectroscopy (using an energy dispersive detector; VEGA 3LMN, INCA ENERGY 450) analyses were conducted on polished thin sections to determine the chemical composition. Morphological details at the IG Komi SC UB RAS (Syktyvkar, Russia) and the fine morphology of nanocrystallites were studied using MIRA3 TESCAN (Tescan, Czech Republic) at the Syktyvkar State University (Syktyvkar, Russia).

The Raman spectra of graphite and related mineral phases were obtained with a high-resolution Raman spectrometer (HR800; Horiba Jobin Yvon, France) at 20°C with a spectral and spatial resolution of approximately 1 cm^{-1} and 1 μm, respectively. For this study, graphite particles from concentrates were used. In situ measurements were conducted on thin

128 polished sections without glass coverings and in cut plates on fresh crashed surfaces of rough
129 samples.

130 The micro- and nanomorphology analyses were performed using an atomic force
131 microscope (AFM; Burleigh ARIS-3300AFM, Germany). Fresh surfaces, obtained by removing
132 the upper layers of graphite with adhesive tape, were studied. The analysis was conducted in
133 standard air atmosphere at 20 °C immediately after the graphite layers were removed.

134 Preliminary studies using transmission electron microscopy (TEM; Tesla BS-500, Czech
135 Republic) were conducted at the Institute of Geology, Komi SC UB RAS (Syktyvkar, Russia) at
136 accelerating voltages of 60 kV and 90 kV. Herein, we used powder specimens prepared by
137 applying ultrasound-treated powder suspensions of chemically separated and ground particles of
138 the carbon substance on perforated carbon films. Further studies were performed at the Central
139 Facility for Electron Microscopy of RWTH Aachen University (Aachen, Germany) with the
140 JEM 2000 FX II (JEOL, Japan), operating at a voltage of 200 kV.

141 GEOLOGICAL POSITION OF GEYSERITES AND TRAVERTINES

142 The studied objects belong to the Ol`khon terrane (Gladkochub et al. 2010), which
143 occupies a part of the western coast of Lake Baikal (the Ol`khon area) and Ol`khon Island. The
144 basement of the Ol`khon terrane is characterized by a metamorphic complex comprising
145 gneisses with silicate and silicate-carbonate compositions, crystalline schists of basic
146 composition, amphibolites with relics of primary magmatic structures, quartzites, marbles,
147 gabbroids, ultramafites, subalkaline and volcanogenic-intrusive series (from monzogabbro to
148 rhyodacite), and rare migmatites and granitoides (Rozen and Fedorovsky 2001). These rocks are

149 composed of diopside, two-pyroxene-hornblende, hornblende-diopside-plagioclase schists, are
150 often garnet-containing, and have plagiogneisses in alternation with quartzites and marbles.
151 High-temperature and post-magmatic metasomatites are widely spread, while metaultramafites
152 and granitoids are less common.

153 The rocks of the complex are characterized by widely varying levels of metamorphism,
154 from green schist to granulite facies. The maximum degree of metamorphism corresponds to the
155 granulite facies, which exist under an estimated pressure range of 7–8 kbar and temperatures of
156 700–850 °C (Petrova and Levitsky 1984). Granulite metamorphism at the Ol`khon terrane
157 occurred in the Early Paleozoic as U-Pb data obtained from zircons from the granulites
158 correspond to 485 ± 5 Ma (Bibikova et al. 1990; Letnikov et al. 1995). The final endogenous
159 events of the Ol`khon terrane include the formation of migmatites and the introduction of
160 syntectonic granite intrusions. Rb-Sr dating of granites showed the age of 449 ± 22 Ma
161 (Serebryansky et al. 1998), which can be considered close to the age of metamorphism and
162 folding (490 ± 10 Ma), although they do not overlap within error.

163 Currently, within the Baikal rift zone (Fig. 1), more than 100 outcrops of Late Quaternary
164 geyserites are known (Sklyarov et al. 2004; 2007; 2014). Further, within the Ol`khon area and
165 Ol`khon Island, travertines are more rare as compared to geyserites. Only two occurrences of
166 travertines have been found (Sklyarov et al. 2007; 2014), appearing as irregularly shaped small
167 bodies among the geyserites of the Krasnaya Gorka area; a travertine vein is exposed in the
168 rocky cliff of the northern tip of Ol`khon Island.

169 The relationships between hydrothermalites and their host rocks were studied and described
170 earlier by Sklyarov et al. (2004, 2007, 2014). The geyserites are represented by eluvial
171 disintegrated blocks (approximately 2 m^3) and less often by bedrock subhorizontal exposures.
172 The bedrock is composed of gneiss, marble, quartzite, amphibolite, granite, ultramafic rocks,
173 and loose Quaternary rocks. The hosting silicate rocks have been found to be completely
174 replaced by the siliceous material of geyserites (Sklyarov et al. 2014).
175 Travertines were not observed to be in original contact with the geyserites, however, the
176 occurrence of their blocks in close proximity to each other has been described (Sklyarov et al.
177 2014).
178 Bedrock outcrops and eluvial disintegrated blocks generally tend to occur in
179 north-northeast-striking faults (which is consistent with the basic structural plan of the region)
180 and are expressed by thick zones of high-temperature milonites and blastomilonites. The
181 formation of these faults is associated with the final stages of Early Paleozoic geological
182 development of the Ol`khon area and Ol`khon Island (Dobrzhinetskaya et al. 1992; Fedorovsky
183 et al. 2005; Gladkochub et al. 2008). During the onset and further development of the Baikal rift
184 zone, the inherited strike-slip faults were periodically repeated, and cases of hydrothermal
185 activity were seemingly associated with them (Sklyarov et al. 2007, 2014).
186 According to radiocarbon measurements (Sklyarov et al. 2007), the age of graphite
187 mineralization within the Ol`khon geyserite vein in the host marble is 23720 ± 425 years
188 (Sklyarov et al. 2007, 2014), and the formation of travertines by calcite radiocarbon exists within
189 the range from 23420 ± 425 to 19550 ± 300 years (radiocarbon calcite dating; Sklyarov et al.
190 2007). Meanwhile, it is necessary to note that graphite mineralization has been previously

191 described in the Early Paleozoic igneous and metamorphic formations of the Ol`khon area, as
192 well as in the later products of tectonic and metasomatic transformation. The latter circumstance
193 requires the consideration of the presence of graphite in the rocks that contain geyserites and
194 travertines when assessing the formation of graphite in the Ol`khon hydrothermalites and its use
195 in genetic reconstruction.

196 ## MICROSCOPIC STUDIES

197 ### Graphite from geyserite

198 Geyserites are fine-grained siliceous (opal-like) rocks. Their porous structure is
199 complicated by spherulitic, globular, microlayer, fibrous, fluidic, looped, and breccia textures
200 (Fig. 2). The carbon content in graphite-containing geyserites varies from 0.01 wt.% to 1 wt.%.
201 Graphite is a prevailing native carbon phase of geyserites. Geyserites contain inclusions of
202 tremolite and fuchsite in equilibrium with the chalcedony matrix (Sklyarov et al. 2014), and are
203 enriched by iron oxides and hydroxides, such as magnetite, hematite, and goethite, as supported
204 by Raman spectroscopy (Figs. 2–4).

205 The graphite in geyserites appears as isolated flakes or is concentrated in aggregates that are
206 several millimeters in size. The carbonaceous matter in the rocks is unevenly distributed,
207 suggesting that the outer zones of globules, spherolites, and surface crusts are the most enriched
208 in particles and clusters of graphite, and spatial conjugation with chalcedonic sites is observed.
209 Graphite particles fill the leaching porous space between inclusions of chalcedony and radially
210 fibrous quartz. An unusual feature of geyserite graphite is the strong splitting at the terminal
211 edges of the plates in cross-section; such formations look like shiefs (Figs. 3–4). Lateral
212 fragmentation has also been observed. Particles of Fe and Mn oxides occur within the nodules

(Fig. 4) where the oxides and graphite co-exist, which usually form at different fO_2 conditions. With reference to the elemental map (Fig. 4b), it is clear that the graphite and the metal oxides belong to different nodule zones indicating different oxygen fugacity during hydrothermalite formation, wherein the highly reductive conditions marked by graphite belong to the central parts of the nodules. Simultaneously, it can be observed that the matrix of silica nodules is clear of impurities in contrast to the general matrix of geyserite, which is strongly enriched in Fe (Figs. 4 g-i); this supports the optical observations shown in Fig. 2c.

Previously, we used an X-ray phase analysis to characterize the graphite of geyserites; it was found to have a high degree of crystallinity (Danilova et al. 2016). The Raman data produced completely analogous results to the spectral characteristics of the reference Ceylon graphite. According to thermal analysis, the temperatures at the onset of the exothermic effect for graphites from geyserites were within 570–710 °C.

Our study of the monomineral fractions of graphite showed that the graphite particles from geyserite were characterized by a pinacoidal habit, which often occurs in rounded and hexagonal forms, and have an irregular flattened shape with sizes from few tenths to a few millimeters.

On the surface of a number of flat-faced graphite particles (approximately 10–15% of the particles studied), we observed very unusual submicrometer-sized crystallites with hexagonal-pyramidal, hexagonal-prismatic habitus, as well as subtrigonal nanocrystallites via SEM (Fig. 5). The size of the crystallites ranged from 50 nm to 1 μm. The layers of submicrometer crystals were parallel or slightly disoriented as they were set close to dissolution zones (Fig. 5c).

Using TEM to achieve a higher resolution, we found that the graphite from geyserites has numerous nanoscale formations with a rounded shape (Fig. 6c), as well as previously described pseudosuperstructures and nanofibers (Danilova et al., 2016). Most often, the graphite particles

in geyserites have rather large regions with a monocrystalline structure (Figs. 6 a–b). Note that the graphite layers did not just shift relative to each other, but collapsed into folds resulting in peculiar wrinkles as well as Moire patterns (Fig. 6 a). This is most likely caused by an exceptionally weak bond between the graphite layers.

Graphite from travertine

Having studied graphite from the natural travertine outcrop at the northern tip of Ol`khon Island, we further investigated the travertines in the outcrop, which exist as a subvertical vein with a thickness of approximately 30 cm in Early Paleozoic gneisses.

According to the description by Sklyarov et al. (2007), travertines are characterized by three consecutive formation phases. The first phase is represented by highly iron-rich cryptocrystalline carbonates of brown color. They are confined to the boundary regions of the vein and are observed as inclusions of irregular shape in the travertines of the second phase, composed of light brownish-yellow fine-crystalline carbonates. The travertines of the first phase contain fragments of silicate rocks, ranging in size from a few millimeters to a few centimeters. They consist mainly of quartz and plagioclase with relatively minor quantities of pyroxene, biotite, apatite, and titanite. The second phase also contains fragments of graphite-containing gneisses and often very highly enriched in graphite with individual grains of quartz and plagioclase; however, the grain sizes do not exceed 1 mm. The third phase, composed of translucent calcite and white and light gray dolomite, is characterized by flow "agate" textures. Herein, travertines contain xenoliths of enclosing silicate rocks with graphite, as well as fragments of the travertines of the first and second phases. This phase fills the cracks in the rocks crossing the travertines of the first and second phases.

Through optical microscopy (Fig. 7) and SEM, we determined that the Ol`khon travertines had not three, but at least five generations (Fig. 8a, Table 1). However, the number of macro- and micro-observations do not correspond well (Table 1). We think that the travertines observed by Sklyarov et al. (2007) are attributed to the aforementioned phases; however, herein, a more detailed portion of travertine formation was observed, allowing us to propose different generations. In general, travertine's variety demonstrates the complicated multiple generations of travertines, attributed to the periodical tectonic activation of the Baikal geyserite paleovalley during the Late Quaternary period. Therefore, it is possible to propose that the earliest travertines generations are iron-free rocks with preferably cryptocrystalline structures without silicate rock fragments and graphite (similar to those in this work). This is followed by the multiple deposited middle stage of iron-rich cryptocrystalline or fine-crystalline travertine abundant in silicate rock fragments and minerals, including graphite, in which multiple fragments of different travertines phases occur (Skyarov et al., 2007 and this work). The latest carbonate generation is represented by Fe-free calcite with 2 wt.% of MgO (this work), which is characterized by a sinter texture. In this study, we did not recognize dolomite as the last portion of carbonate as was reported by Skyarov et al. (2007).

The elemental carbon content in the travertines was approximately 0.1 wt.%. The carbon phases found in these rocks were mainly represented by graphite and, to a lesser extent, by finely dispersed amorphous carbon matter (Danilova et al., 2016). The graphite in travertines is mainly represented by flattened particles of irregular and often elongated shape with sizes ranging from a few micrometers to a few millimeters (Fig. 8 b). These relatively large flattened particles can be bent across the surfaces and are characterized by a large number of overgrowths, which form serrate surfaces in the cross-section, which is similar to the aforementioned geyserite graphite.

283 The graphite particles are distributed in the travertines in an extremely irregular fashion
284 (Figs. 7, 8). Graphite is observed as separate, rather large (> 1 mm), individual particles, as well
285 as in the form of fine-crystalline aggregates filling voids in the travertines of the first and second
286 phases (Fig. 7). The individual graphite particles are confined to xenoliths of enclosing silicate
287 rocks (Fig. 7d) wherein, the travertine matrix contains many graphite particles, most of which
288 are moderately or strongly fragmented.

289 The smallest isolates of amorphous carbon matter are confined to the travertine of the last
290 stage formation, and are represented by flowing zonal crusts, which are shapeless particles that
291 correspond to the spread of the crystallization front of calcite. The abrupt change of carbon-free
292 zones with periodic occurrences of areas substantially enriched in carbon indicates a rapid
293 change in the composition of feeding solutions, which in some cases is manifested by alternating
294 calcite-dolomite zones.

295 In some scenarios, submicrometer crystals are observed on the surface of the isolated
296 graphite particles and have a flat-faced or curved-faced hexagonal-pyramidal and
297 hexagonal-pyramidal-pinacoidal habit (Fig. 9). The size of the crystallites can vary from 50 nm
298 to 1 μm. However, crystallites are more common with sizes between 200 nm and 500 nm along
299 the {002} plane. Upon closer examination, the identified submicrometer crystals, as well as the
300 surface of the substrate on which they are located, exhibit a nanoglobular/blocky character,
301 which can be clearly seen in Figs. 9 b and d where the size scale is approximately 20–30 nm. In
302 addition to the visible hexagonal crystallites, neo formations with non-crystalline forms, which
303 are formed by the fusion of globular-like particles, are observed on the surface of the substrate
304 graphite (Fig. 9a).

305 Although graphite submicrometer crystals have a preferential orientation, some
306 misorientation with respect to each other is still noticeable, especially in the upper parts of the

307 crystallites. Further, many hexagonal subpyramidal submicrometer crystals have peculiar "caps"
308 that also consist of carbon nanoblocks.

309 In addition to the morphology studies from the surface, we also needed to understand the
310 internal structure of the graphite particles. In this regard we have studied the fresh chips of
311 graphite along (002) plane, on which peculiar microscale rounded morphostructures were found
312 (Fig. 10). On the chips of graphite from the geyserites and travertines, we observed a
313 combination of almost perfectly round negative relief forms, with the diameter of the cavities
314 ranging from 100 nm to a few micrometers. Note that sometimes they were co-located so
315 frequently that they formed a peculiar spongy morphostructure (Fig. 10 b) In such areas, the
316 edges of the cavities had irregular outlines. Moreover, the diameters of these relief forms were
317 proportional to the bases of the submicrometer crystals on the surface of the graphite particles of
318 geyserites and travertines.

319 We have never before observed such microstructures in any other type of graphite, including
320 metamorphic, metasomatic, pneumatolytic, and magmatic (Shumilova 2003). These
321 morphostructures occur alongside ideally smooth chips and determine the features of the internal
322 structure of graphite under redeposition conditions during the formation of travertine.

323 **ISOTOPIC STUDIES**

324 Analyses of stable carbon and oxygen isotopes were conducted in samples of
325 graphite-containing geyserites, travertines, and the hydrothermalite-enclosing rocks of the
326 Ol`khon area and the northern edge of Ol`khon Island (Figs. 11, 12, and Table 2). Herein, we
327 evaluated both the gross composition of graphite via chemically isolated concentrates, and the
328 individual particles of graphite extracted directly from some areas of hydrothermalites.

329 Based on our studies on the concentrate, in general, the geyserite graphite had heavy isotope
330 values $\delta^{13}C_{graph}$. The graphite from the remnant of geyserites in gneisses was isotopically the
331 heaviest of all the analyzed samples $\delta^{13}C_{graph}$ (-2.1 to -2.5‰) (Fig. 11, Table 2). Further, the
332 graphite from the geyserite body in marbles was slightly less enriched in heavy isotope $\delta^{13}C_{graph}$
333 (-3.8 to -8.7‰). The values of $\delta^{13}C_{graph}$ in graphite marbles in contact with geyserites were
334 similar (-5.1 to -5.7‰). The measured isotope composition of $\delta^{13}C_{carb}$ carbonate carbon and
335 $\delta^{18}O_{carb}$ oxygen was -2.1 to -2.2‰ and -11.0 to -11.6‰, respectively. Meanwhile,
336 graphite-containing marbles, exposed at some distance from the geyserite outcrop (5 km), were
337 characterized by typical values of the Ol`khon region rocks for $\delta^{13}C_{graph}$ (-1.6 to -2.3‰),
338 carbonate carbon composition - $\delta^{13}C_{carb}$ (1.5–1.6‰), and carbonate oxygen composition -
339 $\delta^{18}O_{carb}$ (-7.1 to -8.8‰). For graphite gneisses and quartzite graphite, the values of $\delta^{13}C_{graph}$
340 ranged from -14.9 to -18.9 ‰ and -10.9 to -12.6 ‰, respectively. The isotopic composition of
341 the individual graphite particles from geyserite lies within the range of -3.8–8.7‰ (Table 2);
342 thus, it can be inferred that the graphite isotopy in geyserite is determined by locally differing
343 values.

344 The study of carbon isotopic composition in the graphite of carbon travertine and calcite
345 oxygen showed that the graphite from travertine had a gross isotope-light composition $\delta^{13}C_{graph}$
346 (-24.3 to -25.7‰), while the carbonate component of the travertines was characterized by a
347 carbon isotopic composition $\delta^{13}C_{carb}$ within -1.1 to -1.9‰ (Fig. 12, Table 2). The $\delta^{18}O_{carb}$ values
348 fall between -11.3 to -13.5‰. Meanwhile, the grain analysis showed that graphite from
349 travertines was very similar to the graphite from gneisses, with a definite tendency toward
350 isotopic composition, which could be associated with the participation of isotopically light
351 hydrocarbons in the process of graphite formation.

RAMAN SPECTROSCOPY

Raman spectroscopy was conducted on the extracted particles of graphite as well as directly "in situ" on the hydrothermalites. The latter turned out to be more informative and allowed us to exclude the possibility of distortion of the structural state of carbonaceous matter that could occur during the chemical extraction of graphite concentrates.

Based on the spectroscopic observations of graphite cross-sections, we revealed not only the characteristics of graphite but also its important paragenetic relationship with the mineral phases. We found micro-inclusions of calcite and chalcedony in geyserite graphite (Fig. 13). Micro-inclusions of quartz and biotite were detected in the travertine graphite, and the presence of hydrocarbons can be assumed owing to a specifically high level of luminescence observed (Fig. 14). The presence of bitumen was confirmed through chemical reactions conducted by chloroform extraction techniques and UV luminescence as described in Danilova et al. (2016).

The Raman spectra indicate that the graphite in both geyserites and travertines is characterized rather by a high degree of crystallinity (French 1964; Tuinstra and Koenig 1970; Wopenka and Pasteris 1993; Tan et al. 2004; Ferrari 2007). In this study, the Raman active $2E_{2g}$ graphite mode, also called the G band, has a position at 1582 cm^{-1}, which corresponds to the standard position of well-ordered graphite. Note that the full-width half-maximum of the G-band has a value of 16–19 cm^{-1}. We did not analyze the characteristics of the D band; this analysis was not useful here because of the significant dependence of a Raman spectrum relative to the crystal orientation in highly ordered graphites. Although, at a qualitative level, note, that while our analyzes have been conducted on the cross sections of graphite plates, i.e., perpendicular to the (002) plane of graphite, the relative intensity of the D band is very insignificant, indirectly indicating a high degree of graphite order in geyserites and travertines.

375 However, in addition to the highly ordered graphite variety in travertines, amorphous
376 carbonaceous matter as fine inclusions was also observed in the travertine of the last generation
377 (Figs. 7 e, f; 14 b).
378

379 **DISCUSSION**

380 Our studies of the graphite in geyserites and travertines of the Ol`khon Paleovalley and
381 Ol`khon Island on Lake Baikal (Eastern Siberia) have provided new mineralogical information,
382 increasing our understanding of the genetic thermal paleoreconstruction of hydrothermalites in
383 the Baikal rift zone as well as other hydrothermal objects through graphite mineralization.
384 Herein, the comparison of hydrothermalite graphite to the carbon mineralization of host
385 rocks was specifically considered; the rocks included gneisses, quartzites, and marbles, that
386 showed graphite mineralization in various degrees. The most useful information was obtained
387 from the isotopic analyses, which showed a correlation between the isotopic composition of
388 geyserite graphite and the graphite of the enclosing marbles, as well as the relationship between
389 travertine graphite and the graphite of the enclosing gneisses. Grain-by-grain analysis revealed a
390 local differentiation of the carbon isotopic composition in graphite that resulted from its initial
391 metamorphic origin, dissolution, and redeposition, with possible isotopic influence from the host
392 carbonates (which displayed different composition in individual particles).
393 Further, we found substantial fragmentation and alteration of the graphite in both geyserites
394 and travertines, which was accompanied by splitting, dissolution, and the appearance of growths
395 on the basal planes and plate edges. Zones of dissolution and growth were clearly observed in
396 optical microscopy observations of thin sections using electron microscopy (Figs. 5, 8, 9). To a
397 certain extent, similar microstructures have been described in Glad et al. (2014), wherein the
398 microstructures were observed on the surface of synthesized graphite produced from gas phase

399 by plasma at low pressure and at the temperature approximately 650 °C, and were observed in
400 natural graphite from Tanzania with crystallite sizes from 50 nm to 800 nm across and up to 1
401 μm along the c-axis. However, the submicrometer crystals found in our study consisted of
402 smaller blocks, approximately 20–30 nm in size, which have never been described before.

403 Although the bulk of graphite from the travertines and geyserites is characterized by a high
404 degree of ordering and belongs to the full-crystal variety after French classification (French
405 1964), we also found amorphous carbon and bitumen among the microscopic carboniferous
406 particles, indicating the heterogeneity of formation conditions of the carbonaceous matter. This
407 could be due to the non-equilibrium conditions of carbon condensation and/or the imposition of
408 carbonaceous mineralization of different origins in hydrothermalites.

409 In addition, bitumen (a hydrocarbon) was detected using Raman spectroscopy, and was
410 found to exist directly in aggregate with graphite (Fig. 14 a), indicating the possible participation
411 of hydrocarbons in hydrothermalite formation. The presence of hydrocarbons could also be the
412 cause of a sharp change in the redox situation, which was observed in the periodical formation of
413 carbon mineralization in the last stage travertines (Figs. 7e, f). This mineralization could be a
414 result of changes in fluid temperature and the corresponding chemical activity in the host
415 metamorphic and sedimentary rocks. Further, possible methane emissions that were described
416 for the different stages of the travertine formation (Lein et al. 2006; Luque et al. 2012) cannot be
417 excluded.

418 In previous works, we have described the presence of single crystalline α-carbyne among
419 native carbons within geyserites (Shumilova et al. 2011; Danilova et al. 2016). This finding was
420 used by Sklyarov et al. for paleothermal reconstruction of the Baikal hydrothermalites (Sklyarov
421 et al. 2014). Following the previously published carbyne data, we suppose that this phase cannot

422 be used as a proven indicator for high temperatures as phases have not been studied in detail and
423 the carbyne position on carbon diagrams (Bundy et al. 1996) is not entirely clear.

424 The graphite in geyserites and travertines is comparable in its degree of structural ordering
425 to graphite from the rocks of the amphibolite facies of metamorphism. The onset temperatures of
426 the exothermic effect for the graphites from geyserites and travertines range between 570–710
427 °C (Danilova et al. 2016), which is a characteristic of graphites from the green shale and
428 epidote-amphibolite facies of regional metamorphism (Ivanova et al. 1974). According to
429 Yardley (1991), this upper limit temperature corresponds to graphite from the amphibolite
430 facies. Such temperature conditions are especially unusual for travertines, for which the
431 temperature regime of formation, as a rule, lies within the range of 20–70 °C (Bargar 1978;
432 Pisarsky 1987; Fouke et al. 2000; Pentecost et al., 2011; Campbell et al., 2015 and others).
433 Sklyarov et al. (2014) used the presence of graphite and carbyne as a justification for the
434 high-temperate nature of the Ol`khon hydrothermalites, estimating a temperature of at least 400
435 °C. However, the features of the studied graphite from travertine and geyserites herein clearly
436 indicate graphite's original genetic relationship with the host rocks, e.g., graphite-containing
437 gneisses and marbles. Therefore, the graphite cannot be used as an unambiguous
438 geothermometer to determine the specifics of the hydrothermalites formation.

439 The mineralogical characteristics of graphite indicate that the travertines and geyserites
440 from the Ol`khon area and Ol`khon Island contain carbonaceous minerals of different origins.
441 The primary graphite in the host rocks during the chemically aggressive hydrothermal
442 processing of gneisses and marbles underwent significant changes associated with
443 defragmentation, partial dissolution, and in situ redeposition that occurred directly on the relict
444 substrates of the primary metamorphic graphite. At the same time, the graphite from travertines
445 and geyserites has very specific characteristics as observed via optical microscopy (Fig. 7b),

446 SEM, TEM, and AFM images (Figs. 5, 6, 8-10); these observations support the presence of
447 newly formed graphite by micro- and submicrometer crystals and unusual micro- and
448 nanostructural features on the surface (Figs. 5, 8, 9), and within the host metamorphic graphite
449 (Figs. 6c, 10).

450 The above presented data explain well the difference between the predominant isotopic
451 composition of graphitic carbon in geyserites and travertines evidenced by the enrichment of a
452 heavy carbon isotope in the geyserites graphite due to the presence of isotopically heavy graphite
453 of marbles and lighter carbon from gneisses associated with travertines (Table 2, Fig. 12). Thus,
454 the travertines and geyserites inherit not only the geochemical features of their host rocks, as
455 indicated in Sklyarov et al. (2007), but also the relict graphite, which generally preserves its
456 initial isotopic composition.

457 In geyserites, a stable silicate framework enables a relatively good preservation of isotopic
458 ratios of graphite (Wada and Suzuki 1983; Dunn and Valley 1992). During the formation of the
459 travertine, isotopic exchange occurred between the graphite of the clastic material in the host
460 rocks and carbon dioxide. Most likely, hydrothermalite graphite has been repeatedly subjected to
461 intense chemical treatment by aggressive hot hydrotherms, possibly with some participation of
462 hydrocarbons, which cause a drastic change in the oxidation-reduction conditions. For example,
463 in the Angel terrace hot springs, Fouke et al (2000) identified five travertine deposition facies
464 that varied in deposition temperature, and $\delta^{13}C$ and $\delta^{18}O$ isotope compositions (Mammoth Hot
465 Springs, Yellowstone National Park, USA). Further, methane emissions could contribute to the
466 prominent depletion of ^{13}C isotope at different stages of travertine formation (Lein et al. 2006;
467 Luque et al. 2012).

468 Moreover, the redox conditions of graphite alteration in the geyserites and travertines could
469 be affected by seasonal temperature fluctuations and spring melt waters, which have a significant

influence on the growth and dissolution of calcite during the formation of travertines (Turi 1986; Naboko et al. 1999; Dilsiz et al. 2004).

The established features of the nanoblock nature of new formations and the fusion of graphite microcrystallites on the surface of graphite particles in the geyserites and travertines indicate a probable mechanism for the coalescence of islands according to Kukushkin and Osipov (1998) under the conditions of free growth from supersaturated solutions and/or from the gas phase. However, the discussion regarding the high-temperature formation of travertines entertained in literature (Sklyarov et al. 2014) cannot be proven with the presence of high crystalline graphite in the samples herein, as they appear, generally, as relict fragments from the host graphite-bearing rocks. Additionally, we must consider the wide range of graphite crystallization temperatures, which reach as low as 98 °C (Dunin-Borkovsky et al. 2000). Thus, these data allow us to conclude that the newly formed redeposited graphite cannot be used as an indicator of high temperature.

Therefore, according to the detailed research on the graphite from the Baikal hydrothermalites paleovalley, we observe a paradox in the graphite nature. After intensive hydrothermal changes of the host metamorphic rocks, only graphite is preserved, thus, the graphite looks to have a hydrothermal nature. Only the provided detailed graphite studies recognize this graphite and understand its deceptive nature. At the same time the real fluid-deposited graphite is represented just by redeposited in situ submicrometer crystallites that overgrow on the surface of the relict metamorphic graphite and between the calcite zones of the last travertine generation. Currently, the fluid deposition of graphite in C–O–H systems occurs at a known high temperature, which is higher than 400 °C with a pressure 2 kbar or greater (Luque et al., 1998; 2009; 2012; Luque and Rodas, 1999). The process of the graphite deposition from C–O–H fluids is completed by the chemical reactions from CO_2-CH_4-H_2O mixtures, such as CO_2

494 $\rightarrow C + O_2$ and $CH_4 + O_2 \rightarrow C + 2H_2O$ (Luque et al., 2012; Ortega et al., 2010). Note that the data
495 complex on the Baikal fluid-deposited graphite formation look different.

496 Considering the surface and subsurface travertine and geyserite formation at atmospheric
497 pressure, it is hard to explain the reason for the thermal conditions for their hot springs being
498 higher than 100 °C, which is the boiling point of water at the atmospheric pressure. Among hot
499 springs, warm (20–40 °C), mesothermal (40–75 °C), and hyperthermal (> 75 °C) varieties are
500 recognized (Pentecost et al., 2003; Renaut and Jone, 2000). Further, travertines are said to
501 deposit at lower temperature conditions, generally below 75 °C, while geyserites more
502 commonly occur at higher temperature conditions (Sklyarov et al, 2014). Thus, we can
503 approximate that the Baikal hydrothermalites (as well as the corresponding graphite
504 redeposition) were formed at atmospheric pressure with a thermal range below 100 °C. For such
505 LPLT-conditions with a large variation from typical C–O–H graphite deposition, the evidence of
506 dissolution and redeposition of the free carbon (relict metamorphic graphite/redeposited
507 graphite) within the C–O–H system indicate that there was a different mechanism involved in the
508 Baikal fluid-deposited graphite formation that did not involve the classic crystallization from a
509 carbon water solution as it has been previously proposed (Dunin-Borkovsky et al. 2000). This
510 novel mechanism put forth herein should be analyzed in detail in a future work. By this work we
511 demonstrate that the PT-conditions for graphite formation within the C–O–H system continue to
512 expand and reveal new information.
513

514 **IMPLICATIONS**

515 In this study, we evaluated the paradox graphite mineralization from the Late Quaternary
516 geyserites and travertines of the Ol`khon area and Ol`khon Island to clarify the genetic value of
517 graphite for hydrothermalite paleoreconstruction. Herein, we demonstrated that the primary

source of graphite in geyserites was enclosing marble, whereas for travertines, it was enclosing gneiss. Metamorphic graphite under the influence of aggressive hydrotherms was forced to partially dissolve and in situ redeposition occurred on the surface of relict graphite particles. The obtained isotope-characteristics and presence of bitumen in our samples indicate non-equilibrium redox conditions of graphite alteration with possible influence from temperature fluctuation and variation in the geochemical nature of the environment with the participation of hydrocarbons. Several mineralogical characteristics, including the micro- and nanostructured features of graphite, can be considered typomorphic for hydrothermalites. Hence, the revealed genetic specifics of graphite crystallized within H_2O-rich LPLT fluid have broadened the established ideas (Luque et al. 1998, 2012; Jaszczak et al. 2007) on typomorphism and diversity of carbon mineralization in connection with fluidogenic objects. The redeposition of the graphite within the Baikal Quaternary geyserites and travertines supported by earlier experimental LPLT synthesis in aqueous solutions allow for the consideration of a new natural mechanism of LPLT graphite formation in a C–O–H system, that is, crystallization from carbon water solution, which should be further detailed in future studies.

ACKNOWLEDGMENTS

The authors thank E.V. Sklyarov for providing the samples for research and for the scientific advice. E.M. Tropnikov, I.V. Smoleva, A. Sologubenko, V.N. Filippov, V.A. Radaev, G.N. Kablis, G.N. Modyanova, N.A. Priezzheva, V.A. Ponomarchuk, B.A. Makeev, and N.V. Nartova are acknowledged for their assistance in the analyses.

FUNDING

The work was supported by the projects: NIR GR # AAAA-A17-117121270036-7; Basic

Research Program IX.130, project # 0346-2019-0003.

Author Contributions: Tatyana Shumilova provided the idea for the study, conducted all mineralogical investigations, collected and interpreted the instrumental data, and wrote the manuscript. Yulia Danilova conducted the petrographic and geological analyses, participated in data interpretation, and wrote the manuscript. Joachim Mayer performed the TEM studies and edited the manuscript. Sergey Isaenko measured the Raman spectra, and Boris Danilov performed the geological analysis. Vasily Ulyashev assisted in the high resolution SEM studies.

Conflicts of interests: The authors declare no conflict of interest.

REFERENCES CITED

Altunel, E., and Hancock, P.L. (1993) Morphology and structural setting of Quaternary travertines at Pamukkale, Turkey. Geological Journal, 28, ¾, 335–346.

Bargar, K. (1978) Geology and thermal history of Mammoth Hot Springs, Yellowstone National Park, Wyoming: U.S. Geological Survey Bulletin, 1444, 1–54.

Bibikova, E.V., Karpenko, S.F., Sumin, and L.M. (1990) U-Rb, Sm–Nd, and K–Ar Age of Metamorphic and Igneous Rocks of the Ol'khon Region (Western Baikal Region), In Precambrian Geology and Geochronology of the Siberian Craton and Its Fold Framework, p. 170–183. Nauka, Leningrad (in Russian).

Bundy, F.P., Basset, W.A., Weathers, M.S., Hemley, R.J., Mao, H.K., and Goncharov, A.F. (1996) The pressure-temperature phase and transformation diagram for carbon: updated

through 1994. Carbon, 34, 2, 141–153.

Campbell, K.A., Guido, D., Gautret, P., Foucher, F., Ramboz, C. et. al. (2015) Geyserite in Hot-Spring Siliceous Sinter: Window on Earth's Hottest Terrestrial (Paleo) environment and its Extreme Life. Earth-Science Reviews, Elsevier, 148, 44–64.

Crossey, L.J., Karlstrom, K.E., Springer, A.E., Newell, D., Hilton, D.R., and Fischer, T. (2009) Degassing of mantle-derived CO2 and He from springs in the southern Colorado Plateau region — Neotectonic connections and implications for groundwater systems. GSA Bulletin, 121, 7/8, 1034–1053.

Danilova,, Yu.V, Shumilova, T.G., Mayer, J., and Danilov, B.S. (2016) Conditions and Formation Mechanism of Carbon Phases in Late Quarternary Geyzerites and Travertines of Ol'khon Area and Ol'khon Island (Baikal Rift Zone). Petrology, 24, 1, 35–48.

Dilsiz, C., Marques, J.M.M., and Carreira, P.M.M. (2004) The impact of hydrological changes on travertine deposits related to thermal springs in the Pamukkale area (SW Turkey). Environmental Geology, 45, 808–817

Djokic, T., Van, Kranendonk, M.J., Kathleen, A.C., Malcolm, R.W., and Colin, R.W. (2017) Earliest signs of life on land preserved in ca. 3.5 Ga hot spring deposits. Nature Communications, 8, 15263. https://doi.org/10.1038/ncomms15263.

Dobrzhinetskaya, L.F., Molchanova, T.V., Sonyushkin, V.E., Likhachev, A.B., and Fedorovskii, V.S. (1992) Napped and strikeslip ductile deformations of the Ol'khon Region metamorphic complex (western Baikal region). Geotektonika, 2, 58–71.

Duke, E. F. and Rumble, D. (1986). Textural and isotopic variations in graphite from plutonic rocks, South-Central New Hampshire. Contributions to Mineralogy and Petrology, 93(4), 409–419.doi:10.1007/bf00371711

586 Dunin-Barkovsky, R.L., Dunin-Barkovsky, A.R., Drozdova, O.V., Kidyarov, B.I., Kolyago,
587 S.S., Kozhbakhteyev, E.M., Lisitsina, E.E., Mar`in, A.A., and Slovtsov, I.B. (2000)
588 Low-Temperature Growth of Diamond Seedings in Acid Solutions. Chemistry for
589 Sustainable Development, 8, 147–153.
590 Dunn, S., and Valley, J. (1992) Calcite-graphite isotope thermometry: a test for
591 polymetamorphism in marble, Tudor gabbro aureole, Ontario, Canada. Journal of
592 Metamorphic Geology, 10, 4, 487–501.
593 Fedorovsky, V.S., Donskaya, T.V., Gladkochub, D.P., Khromykh, S.V., Mazukabzov, A.M.,
594 Mekhonoshin, A.S., Sklyarov, E.V., Sukhorukov, V.P., Vladimirov, A.G., Volkova, N.I.,
595 and Yudin, D.S. (2005) The Ol'khon collision system (Baikal region) in Structural and
596 tectonic correlation across the Central Asia orogenic collage: northeastern segment. In
597 Guidebook and Abstract Volume of the Siberian Workshop IGCP-480, Sklyarov EV,
598 Ed., Print. IEC SB RAS: Irkutsk.
599 Ferrari, A. (2007) Raman spectroscopy of graphene and graphite: Disorder, electron–phonon
600 coupling, doping and nonadiabatic effects. Solid State Communications, 143, 47–57.
601 Fouke, B., Farmer, J., Marais, D., Pratt, L., Sturchio, N., Burns, P., and Discipulo, M. (2000)
602 Depositional facies and aqueous-solid geochemistry of travertine-depositing hot springs
603 (Angel Terrace, Mammoth Hot Springs, Yellowstone National Park, U.S.A.). Journal of
604 Sedimentary Research, 70, 3, 565–585.
605 Fraedrich W., Heidari N. (2019) Iceland from the West to the South. GeoGuide. Springer,
606 Nature, Switzerland AG.
607 French, B.M. (1964) Graphitization of organic material in a progressively metamorphosed
608 Precambrian iron formation. Science, 146, 3646, 147–153.
609 Gibert, R.O., Taberner, C., Sáez, A., Giralt, S., Alonso, R.N., Edwards, R.L., and Pueyo, J.J.

(2009) Igneous Origin of CO2 in Ancient and Recent Hot-Spring Waters and Travertines from the Northern Argentinean Andes. Journal of Sedimentary Research, 79, 8, 554–567.

Glad, X., Poucques, L., Jaszczak, J.A., Belmahi, M., Ghanbaja, J., and Bougdira, J. (2014) Plasma synthesis of hexagonal-pyramidal graphite hillocks. Carbon, 76, 330–340.

Gladkochub, D.P., Donskaya, T.V., Fedorovsky, V.S., Mazukabzov, A.M., Larionov, A.N., and Sergeev, S.A. (2010) The Olkhon metamorphic terrane in the Baikal region: An Early Paleozoic collage of Neoproterozoic active margin fragments. Russian Geology and Geophysics, 51, 5, 447–460.

Gladkochub, D.P., Donskaya, T.V., Wingate, M.T.D., Poller, U., Kröner, A., Fedorovsky, V.S., Mazukabzov, A.M., Todt, W., and Pisarevsky, S.A. (2008) Petrology, geochronology, and tectonic implications of c. 500 Ma metamorphic and igneous rocks along the northern margin of the Central-Asian orogen (Olkhon Terrane, Lake Baikal, Siberia) Journal of the Geological Society of London, 165, 1, 235–246.

Harris, A.C., White, N.C., McPhie, J., Bull, S.W., Line, M.A., Skrzeczynski, R., Mernagh, T.P., and Tosdal, R.M. (2009) Early Archean hot springs above epithermal veins, North Pole, Western Australia: new insights from fluid inclusion microanalysis. Economic Geology, 104, 6, 793-814.

Ivanova, V.P., Kasatov, B.K., Krasavina, and T.N. (1974) Thermal analysis of minerals and rocks. Nedra, Leningrad (in Russian).

Jaszczak, J.A., Dimovski, S., Hackney, S.A., Robinson, G.W., Bosio, P., and Gogotsi, Yu. (2007) Micro- and nanoscale graphite cones and tubes from Hackman Valley, Kola Peninsula, Russia. The Canadian Mineralogist, 45, 2, 379–389.

632 Jones, B., and Renaut, R.W. (2003) Hot spring and geyser sinters: the integrated product of
633 precipitation, replacement, and deposition. Canadian Journal of Earth Sciences, 40, 11,
634 1549–1569.
635 Kukushkin, S.A., and Osipov, A.V. (1998) Condensation processes of thin films. Success of
636 physical sciences, 168, 10, 1083–1116 (in Russian),
637 Lein, A.Yu,, Bogdanov, Yu.A, Grichuk, D.V., Rusanov, I.I. and Sagalevich, A.M. (2006)
638 Geochemistry of hydrothermal solutions from 9°50′ N at the East Pacific Rise (EPR)
639 within twelve years after the eruption of a submarine volcano. Geochemistry International,
640 44, 7, 690–703.
641 Letnikov, F.A., Khalilov, V.A., Savel'eva, and V.B. (1995) Isotopic Dating of Endogenic
642 Processes in the Ol'khon Region. Doklady Earth Sciences, 344, 1, 96–100.
643 Luque, F.J., Crespo-Feo, E., Barrenechea, J.F., Ortega, L. (2012) Carbon isotopes of graphite:
644 Implications on fluid history. Geoscience Frontiers, 3, 2, 197–207.
645 Luque, F.J., Pasteris, J.D., Wopenka, B., Rodas, M., and Barrenechea, J.F. (1998) Natural
646 fluid-deposited graphite: mineralogical characteristics and mechanisms of formation.
647 American Journal of Science, 298, 471–498.
648 Lund, J., Freeston, D.H., and Boyd, T.L. (2005) World-wide direct uses of geothermal energy.
649 Proceedings of World Geothermal Congress, Antalya, Turkey.
650 http://citeseerx.ist.psu.edu/viewdoc/download?doi=10.1.1.536.1578&rep=rep1&type=pdf
651 Minissale, A,, Kerrick, D.M., Magro, G., Murrell, M.T., Paladini, M., Rihs, S., Sturchio, N.C.,
652 Tassi, F., and Vaselli, O. (2002) Geochemistry of Quaternary travertines in the region
653 north of Rome (Italy): structural, hydrologic and paleoclimatic implications. Earth and
654 Plane Science Letters, 203, 2, 709–728.
655 Naboko, S.I., Lugovaya, I.P., and Zagnitko, V.N. (1999) The isotope composition of oxygen and

656 carbon in modern travertines and Kamchatka geyserites. Mineralogical journal, 21, 5/6,
657 33–39 (in Russian).
658 Omelon, C.R., Pollard, W.H., and Andersen, D.T. (2006) A geochemical evaluation of
659 perennial spring activity and associated mineral precipitates at Expedition Fjord, Axel
660 Heiberg Island, Canadian High Arctic. Applied Geochemistry, 21, 1–15.
661 Pisarsky, B.I. (1987) Patterns of formation of underground flow of Lake Baikal. Nauka,
662 Novosibirsk (in Russian)
663 Pentecost, A. (1995) Geochemistry of carbon dioxide in six travertine-depositing waters of
664 Italy. Journal of Hydrolody, 167, 263–278.
665 Pentecost, A. (2005) Travertine. Springer-Verlag, London. https://www.academia.edu/8180604
666 Pentecost, A., and Viles, H.A. (1994) Review and Reassessment of Travertine Classification.
667 Géographie physique et Quaternaire, 48, 3, 305–314.
668 Petrova, Z.I., and Levitsky, V.I. (1984) Petrology and Geochemistry of Granulite Complexes of
669 the Baikal Region. Nauka, Novosibirsk (in Russian).
670 Renaut, R.W., Owen, R.B., and Ego, J.K. (2008) Recent changes in geyser activity at Loburu,
671 Lake Bogoria, Kenya rift valley. GOSA Transact, 10, 4–14.
672 Renaut, R.W., Owen, R.B., Jones, B., Tiercelin, J-J., Ego, J.K., and Konhauser, K.O. (2013)
673 Impact of lake-level changes on the formation of thermogene travertine in continental
674 rifts: evidence from Lake Bogoria, Kenya rift valley. Sedimentology, 60, 428–468.
675 Rozen, O.M., and Fedorovsky, V.S. (2001) Collisional granitoids and stratification of the Earth's
676 crust (examples of Cenozoic, Paleozoic and Proterozoic collisional systems). In:
677 Proceedings GIN RAS. Mir, Moscow (in Russian).

678 Serebryansky, E.P., Kostitsyn, Yu..A., Fedorovsky, V.S., and Vladimirov, A.G. (1998)
679 Comparative isotopic studies of granites and metamorphic rocks of the Olkhon region. In:
680 XU Symposium on Geochemistry of Isotopes. GEOKHI RAS, Moscow.
681 Shumilova, T.G. (2003) Mineralogy of native carbon. Ural Branch of RAS press: Ekaterinburg,
682 Russia, 316 p. (in Russian).
683 Shumilova, T.G., and Danilova, Yu.V. (2009) New genetic types of graphite in connection
684 with travertines. Doklady Earth Sciences, 428, 2, 1171–1173.
685 Shumilova, T.G., Danilova, Yu.V., Gorbunov, M.V., and Isaenko, S.I. (2011) Natural
686 Monocrystalline α-Carbyne. Doklady Earth Sciences, 436, 1, 152–154.
687 Shumilova, T.G., Isaenko, S.I., and Yashin, N.V. (2018) Structure and mineral characteristics
688 of travertine object Vas`kin Klyuch (Sukhona River, Vologda District). Mineralogy, 4, 4,
689 119–129 (in Russian).
690 Sklyarov, E.V., Fedorovskii, V.S., Kulagina, N.V., Sklyarova, O.A., and Skovitina, T.M.
691 (2004) The Late Quaternary “Geyser Valley” in the western flank of the Baikal Rift
692 (Ol’khon Region). Doklady Earth Sciences, 395A, 3, 324–327.
693 Sklyarov, E.V., Fedorovskii, V.S., Sklyarova, O.A., Skovitina, T.M., Danilova, Yu.V., Orlova,
694 L.A., and Ukhova, N.N. (2007) Hydrothermal Activity in the Baikal Rift Zone: Recent Hot
695 Springs and Deposits of Paleothermal Waters. Doklady Earth Sciences, 412, 2, 101-105.
696 Sklyarov, E.V., Skovitina, T.M., Sklyarova, O.A., Kotov, A.B., Tolmacheva, E.V., and
697 Velikoslavinskii, S.D. (2014) Late Quaternary high-temperature geyserites in the Ol’khon
698 area, Baikal rift zone: Petrography, mineralogy, chemical composition, and genesis.
699 Petrology, 22, 6, 536-546.

Tan, P.H., Dimovski, S., and Gogotsi, Y. (2004) Raman scattering of non-planar graphite: arched edges, polyhedral crystals, arched edges, polyhedral crystals. Phil. Trans. R Soc. Lond. A, 362, 2289–2310.

Tatarinov, A.V., Yalovik, L.I., Danilova, E.V., and Namsaraev, Z.B. (2006) Participation of Microorganisms in the Formation of Travertines and Sapropelite Kerogen in Sediments of Thermal Carbonic Waters in the Baikal Rift Zone. Doklady Earth Science,s 411A, 9, 1435–1438.

Tuinstra, F. and Koenig, J.L. (1970) Raman Spectrum of Graphite. Journal of Chemical Physics, 53, 1126–1130.

Turi, B. (1986) Stable isotope geochemistry of travertines. Handbook of environmental isotope geochemistry, Elsevier: Amsterdam.

Van Kranendonk, M.J. (2006) Volcanic degassing, hydrothermal circulation and the flourishing of early life on Earth: a review of the evidence from c. 3490-3240 Ma rocks of the Pilbara Supergroup, Pilbara Craton, Western Australia. Earth Science Reviews, 74, 3-4, 197–240.

Wada, H., and Suzuki, K. (1983) Carbon isotopic thermometry calibrated by dolomite-calcite solvus temperatures. Geochimica et Cosmochimica Acta, 47, 4, 697–706.

Wopenka, B., and Pasteris, J.D. (1993) Structural characterization of kerogens to granulite-facies graphite: applicability of Raman microprobe spectroscopy. The American Mineralogist, 78, 5/6, 533–557.

Yardley, B.W.D. (1991) An introduction to metamorphic petrology. Longman Scientific and Technical, New York.

FIGURE CAPTIONS

FIGURE 1. Geographic position of Lake Baikal and the Ol'khon Island (Russia) (b) on the Google map (a); fragment of the Baikal rift zone on the geological scheme (c). Legend: 1 – Siberian craton; 2 – the Ol'khon Area and the Island Ol'khon system of shear plates formed igneous and metamorphic complexes; 3 – faults (3a) the boundary of the Siberian craton and the Ol'khon Area, (3b) the main shift zone of the region; 4 – outcrops with (4a) geyserite and (4b) travertine; 5 –corresponding geyserites (5a) and travertine (5b) objects with graphite (sampling sites).

FIGURE 2. Graphite particles in different areas of geyserites of a polished section: (a, b) Graphite aggregates in chalcedony nodules. (a) overview of a nodule with graphite inclusion. (b) Magnified view of the section demarcated by the rectangle in (a). (c) Graphite in general geyserite matrix. (d) A graphite aggregate inclusion inside a closed chalcedony nodule.

FIGURE 3. Morphological features of graphite aggregates and iron hydroxide particles in geyserite. (a) Aggregate of graphite plates in cross-section (center), where hydroxides in the main microglobular matrix of the geyserite fill the gaps between microglobules (brown). (b) Particles of hematite (indicated by arrows) surrounded by a halo of iron hydroxides. (c, d) Sheaf-like graphite particles. (e, f) fragmented graphite particles in geyserite. Note: (a – c, e) are the optical images in transmitted light, with parallel polarizers and (d, f) are the optical images in transmitted light, with crossed polarizers.

FIGURE 4. Electron microscopy images of graphite-containing geyserite. (a–f) Chalcedony nodule with graphite-containing core. (g–i) general geyserite matrix. Note that (a) is a BSE image; (b–i) are the elemental maps wherein (b, g) are the multi-element maps and (c–f, h, i) are the individual element maps.

747 **FIGURE 5.** Scanning electron microscopy (SEM) images (in the secondary electron mode
748 (SE)) of graphite from geyserite showing dissolution and new-growth regions. (a) Graphite
749 particle overview; the area demarcated by the square is the region considered for detailed study
750 (b–d are the magnified images of the area demarcated in (a)). (b) The region with newly formed
751 hexagonal subprismatic and tiny pyramidal graphite crystallites. (c) The region with graphite
752 dissolution. (d) Subtrigonal and smooth pyramidal graphite crystals, micro- and submicrometer
753 in size.

754 **FIGURE 6.** Transmission electron microscopy (TEM) data of graphite from (a–b)
755 geyserite and (d–f) and travertine. (a) Bright field image (BF) of single crystalline graphite
756 particle with layer wrinkles (white arrows) and Moire fringes (black arrows). (b) Electron
757 diffraction pattern (ED) of the graphite in (a). (c) Rounded graphitic nanosized nuclear particles
758 of newly-forming graphite. (d) Typical shapes of crushed graphite particles with rounded
759 fragments in chips. (e) A fragment of oriented growth of graphite nanocrystals in (002) direction
760 and the corresponding ED pattern. (f) The BF images of (a, c, d, and e).

761 **FIGURE 7.** Optical images of graphite-containing travertine in (a, c) reflected (skew
762 angle) and (b, d–f) transparent light. (a) Travertine overview with different travertine
763 generations. (b) Cross-section of a graphite particle within travertine matrix (tooth-like surface,
764 with overgrowths). (c) Boundary between the latest Fe-free travertine generation and an earlier
765 travertine. (d) The fragment of graphite-rich gneiss within travertine. (e) The carbonate of the
766 last generation with microcrystalline graphite. (f) Magnified image of (e).

767 **FIGURE 8.** SEM images of travertine and graphite particles chemically extracted from
768 the host travertine. Travertine of several generations (I-V), graphite inclusions are indicated with
769 arrows (a). (a) BS mode and (b–g) secondary electron (SE) mode where (b) shows shape of
770 graphite particles, (c) shows an individual particle with the studied region demarcated with a

771 square, (d) magnified view of the region demarcated (c). (e) Regions with dissolution (indicated
772 with arrows) and newly formed graphite crystallites on the {002} planes. (f) Newly formed
773 graphite crystallites on the {002} plane edges and regions with dissolution (indicated with
774 arrows). (g) Newly formed graphite crystallites on the {002} plane, regions with dissolution, and
775 {002} plane relics (indicated with arrows).

776 **FIGURE 9.** SEM images in the SE mode. (a) Micro- and submicrometer features of newly
777 formed graphite from travertine at the edge of the seed graphite plate. (b) Growth of nanoblock
778 sub-hexagonal micro- and submicrometer crystals on the surface of the graphite seed plate. (c)
779 Tight growth of nanoblock micro- and submicrometer crystals along the seed graphite plate
780 edge. (d) Nanoblock sub-hexagonal microcrystallite.

781 **FIGURE 10.** Atomic force microscope (AFM) data of fresh crushed surfaces of graphite
782 from (a, b) geyserite and (c, d) travertine. (a, c, d) have rounded morphology while (b) has a
783 sponge-like morphology.

784 **FIGURE 11.** Isotope composition of graphite and carbonates in geyserites, travertines,
785 and their host rocks.

786 **FIGURE 12.** Carbon and oxygen isotopic composition of carbonates in hydrothermalites
787 and their host rocks.

788 **FIGURE 13.** Raman spectra of graphite "in situ" in geyserite in perpendicular direction to
789 {002} of (a) pure graphite, (b) graphite with calcite inclusion (156 cm^{-1}, 281 cm^{-1}, and 1087
790 cm^{-1}), and (c) graphite with chalcedony inclusion (130 cm^{-1}, 210 cm^{-1}, 465 cm^{-1}, and 503 cm^{-1}).

791 **FIGURE 14.** Raman spectra of graphite "in situ" in travertine in crosscut direction to
792 {002} of the graphite particle where (a) is the spectrum from hydrocarbon (luminescence) and
793 quartz (464 cm^{-1}) impurities within graphite, (b) is graphite with biotite inclusion (194, 558, 962
794 cm^{-1}), probably with hydrocarbon (luminescence), and (c) is pure graphite.

Table 1 General characteristics of travertines generations

Generations of travertines at micro-observations (this work, corresponding to the Fig. 8a)	Macro-view generations (phases) of travertines (Sklyarov et al., 2007)
I generation - cryptocrystalline carbonate, free of fragments of silicate rocks and minerals, free of graphite	**I phase** is presented with very iron-rich cryptocrystalline carbonates of brown color; contains fragments of silicate rocks and minerals.
II generation – fine-crystalline carbonate, rich by fragments of silicate rocks and minerals, includes graphite particles	
III generation - iron-rich fine-crystalline carbonates of brown color, with minerals fragments, without fragments of silicate rocks and graphite; includes fragments of the generation I and II.	
IV generation - light brownish-yellow fine crystalline carbonates, contain fragments of the III generation, numerous fragments of graphite-containing gneisses, enriched in graphite, and individual grains of quartz and plagioclase	**II phase** consists of light brownish-yellow fine crystalline carbonates; contain fragments of the phase I, graphite-containing gneisses, graphite, individual grains of quartz and plagioclase.
V generation is characterized with white calcite with sinter ("agate") texture, free of any rock and mineral inclusions, sometimes graphite micro-inclusions between calcite zones.	**III phase** composed of translucent calcite, white and light gray dolomite, has "agate" textures; contain fragments of silicate rocks with graphite, fragments of the travertine I and II phases; fill cracks crossing the travertines of the first and second phases.

Table 2 Isotope composition of carbon and oxygen in host geyserites and travertines and graphite carbon

No	Specimen	Specimen type	Specimen characteristic	$\delta^{13}C_{graph}$,‰ (PDB)	$\delta^{13}C_{carb}$,‰ (PDB)	$\delta^{18}O_{carb}$,‰ (PDB)	$\delta^{18}O_{carb}$,‰ (SMOW)
Geyserites and host rocks							
1	57/05-01	Chemical concentrate	Geyserite with graphite in gneisses	-2.1			
2	57/05-02	–"–		-2.5			
3	57/05	–"–		-4.5			
4	Skl05-gn	–"–	Geyserite with graphite in marbles	-8.7			
5	Skl05-g1	–"–		-7.3			
6	Skl05-g2	–"–		-3.8			
7	Skl05	–"–		-6.0			
8	65/06-m1	–"–	Marble with graphite, on the contact with geyserites	-5.7	-2.2	-11.0	19.5
9	65/06-m2	–"–		-5.1	-2.1	-11.6	18.5
10	65/06-1	Grain	Graphite from marble enclosing geyserite	-7.91			
11	65/06-2	–"–	–"–	-8.39			
12	65/06-3	–"–	–"–	-7.97			
13	65/06-4	–"–	–"–	-7.28			
14	65/06-5	–"–	–"–	-6.82			
15	1124/94	Chemical concentrate	Marble with graphite	-2.3	1.5	-8.8	21.8
16	1126/94	–"–		-1.6	1.6	-7.1	23.5
17	66/06	–"–	Quartzite with graphite	-12.6			
Travertines and host rocks							
18	B-1	Chemical concentrate	Quartzite with graphite	-10.9			
19	G2-1	–"–	Travertine with graphite	-24.3	-1.1	-11.3	19.2
20	G2-1k	–"–	Travertine	-	-1.9	-13.5	17.3
21	G2-2	–"–	Travertine with graphite	-25.7	-1.8	-12.7	17.4
22	G2-1-6	Grain	Graphite from gneiss fragment in travertine	-7.69			
23	G2-1-7	–"–	–"–	-9.12			
24	G2-1-8	–"–	–"–	-12.08			
25	G2-1-9	–"–	–"–	-10.67			
26	G2-1-10	–"–	–"–	-17.03			

27	G2-1-11	Grain	Graphite from travertine matrix	-10.08
28	G2-1-12	–”–	–”–	-11.04
29	G2-1-13	–”–	–”–	-15.04
30	G2-1-14	–”–	–”–	-16.77
31	G2-1-15	–”–	–”–	-18.66

* Conducted at IG FRC Komi SC UB RAS, Syktyvkar, analyst I.V. Smoleva. ** Conducted at UIGGM SB RAS, Novosibirsk, V.A. Ponomarchuk.

Figure 1

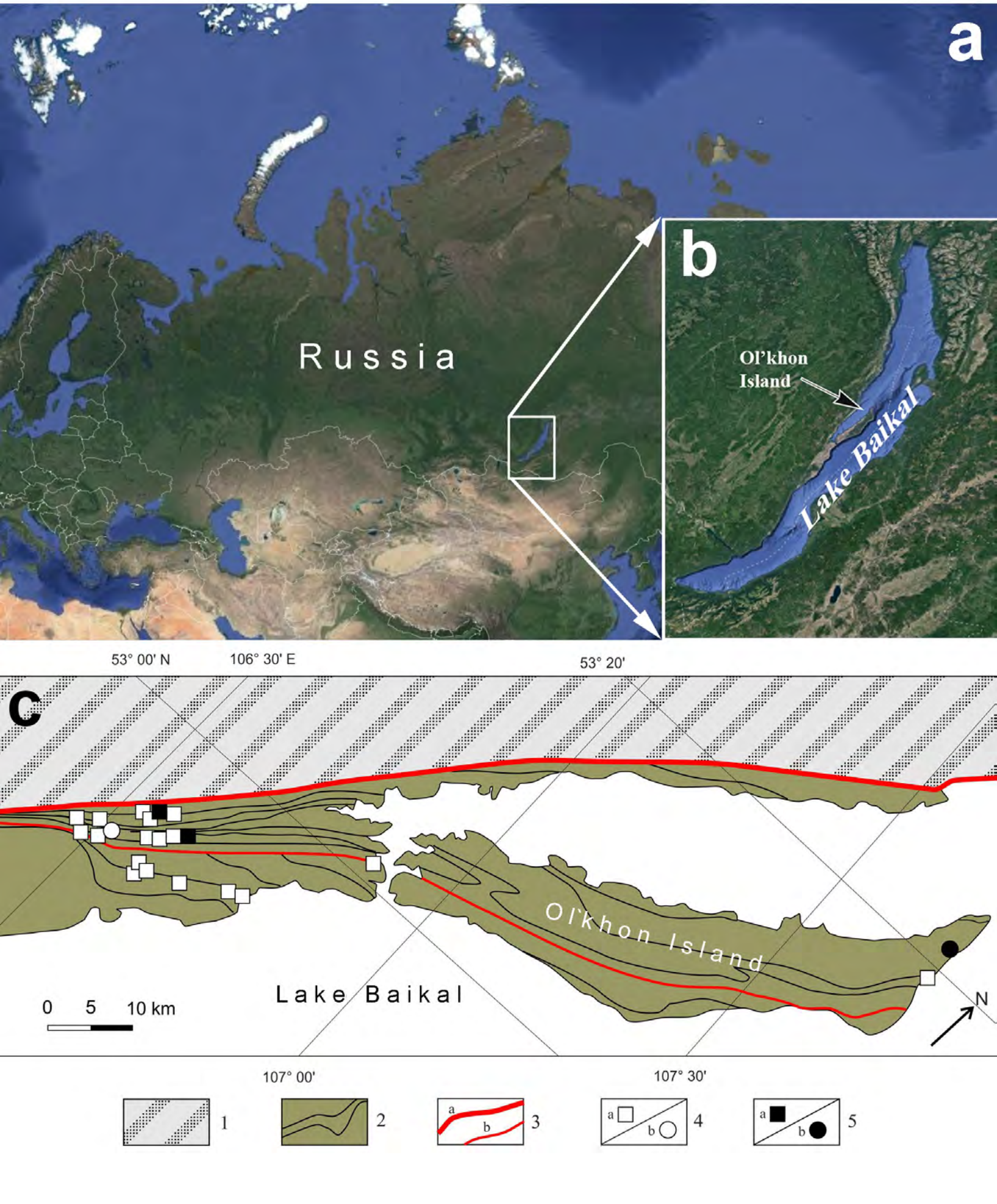
a
Russia
b
Ol'khon
Island
Lake Baikal
53° 00' N
106° 30' E
53° 20'
c
Ol'khon Island
Lake Baikal
0 5 10 km
N
107° 00'
107° 30'
1
2
a
b
3
a
b
4
a
b
5

Figure 2

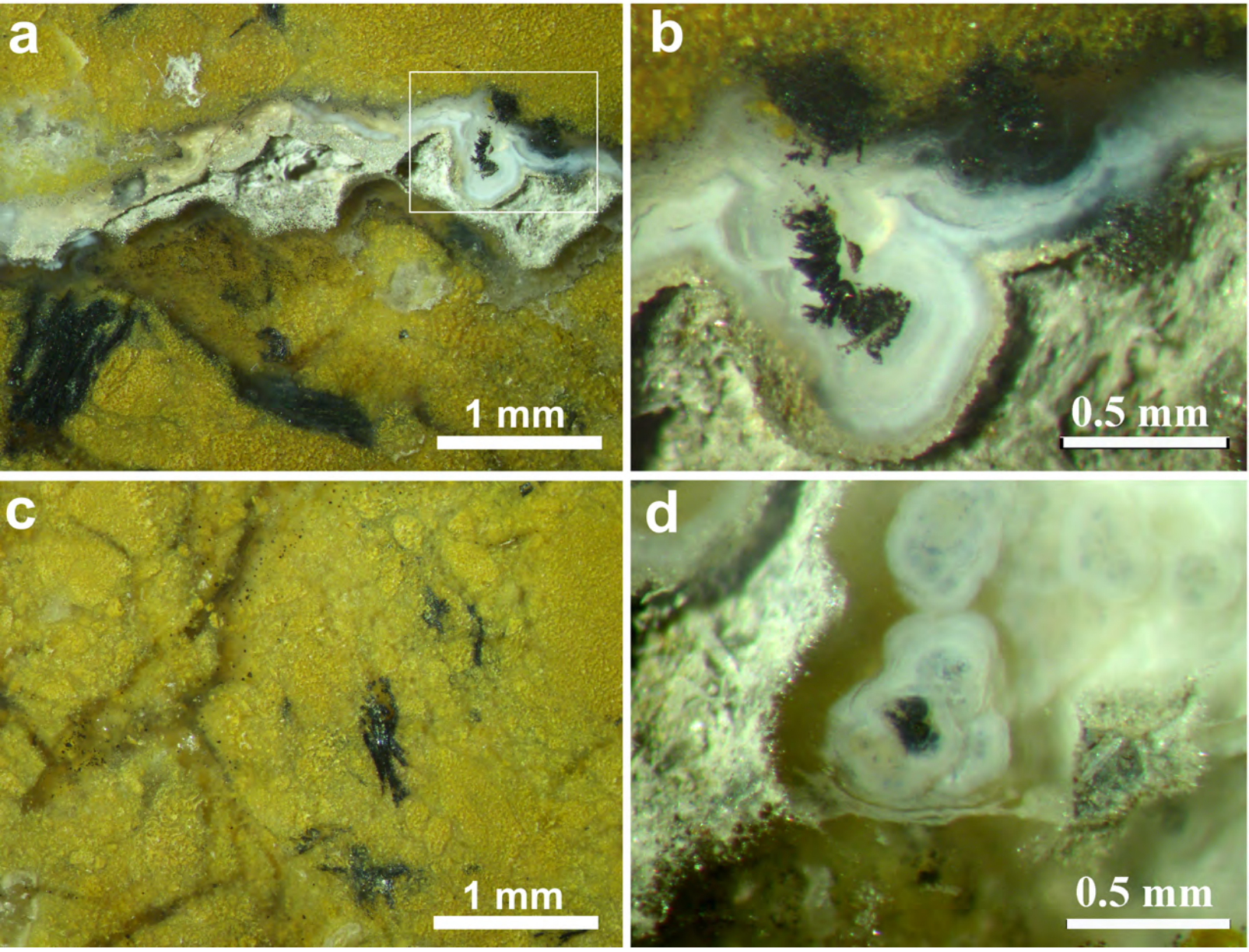

Figure 3

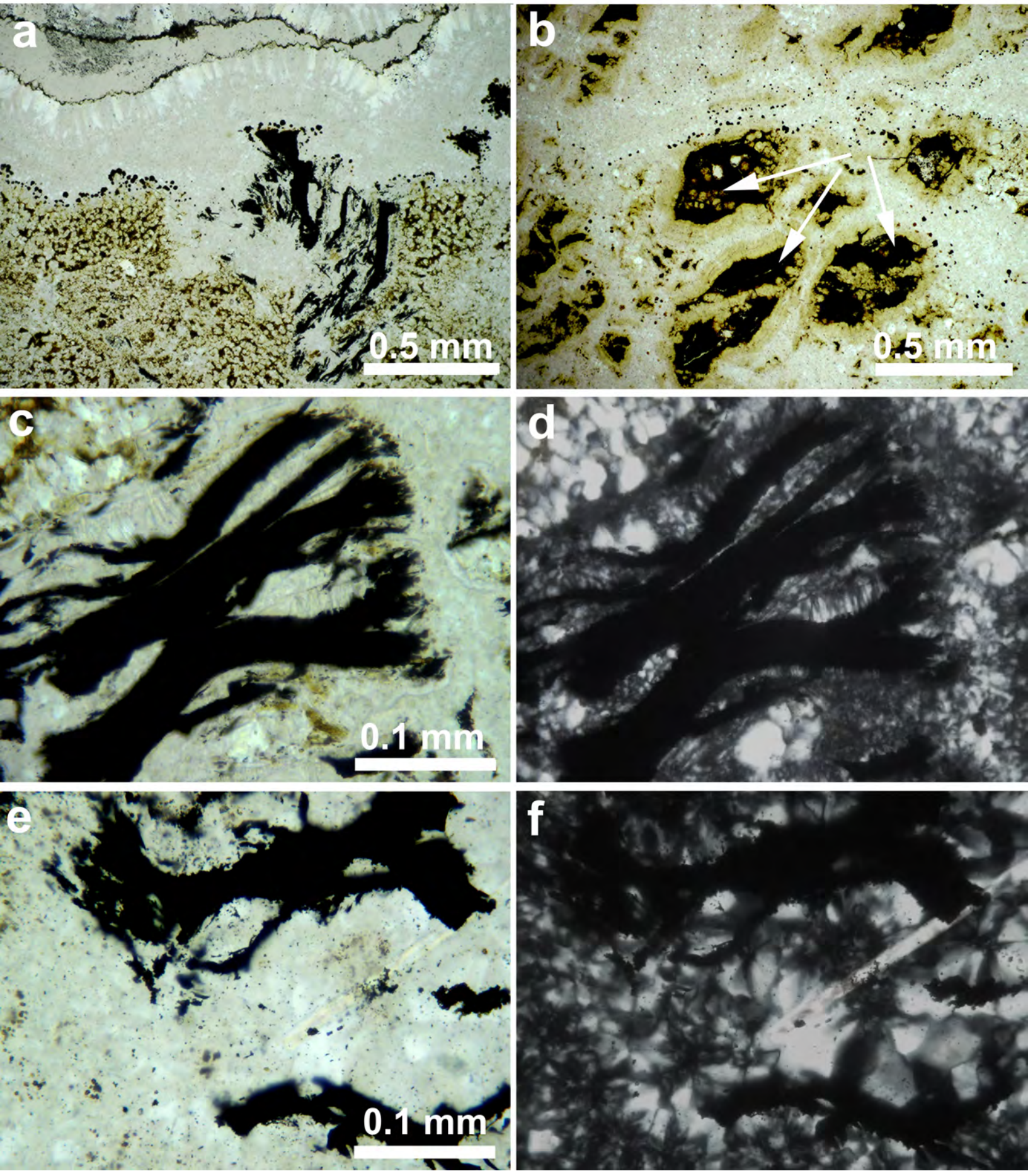

Figure 4

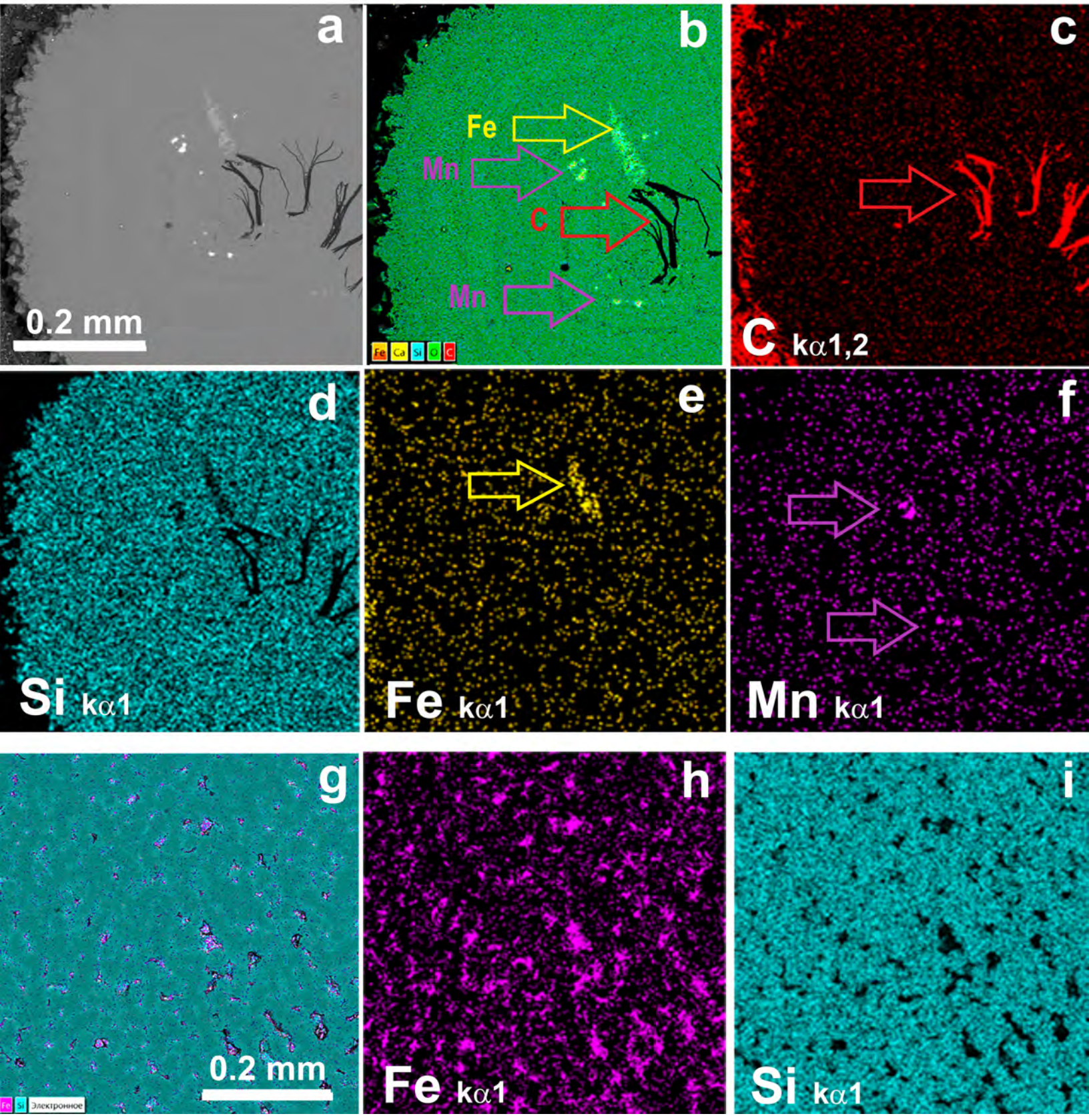
a
0.2 mm
b
Fe
Mn
C
Mn
Fe Ca Si O C
c
C kα1,2
d
Si kα1
e
Fe kα1
f
Mn kα1
g
0.2 mm
Fe Si Электронное
h
Fe kα1
i
Si kα1

Figure 5

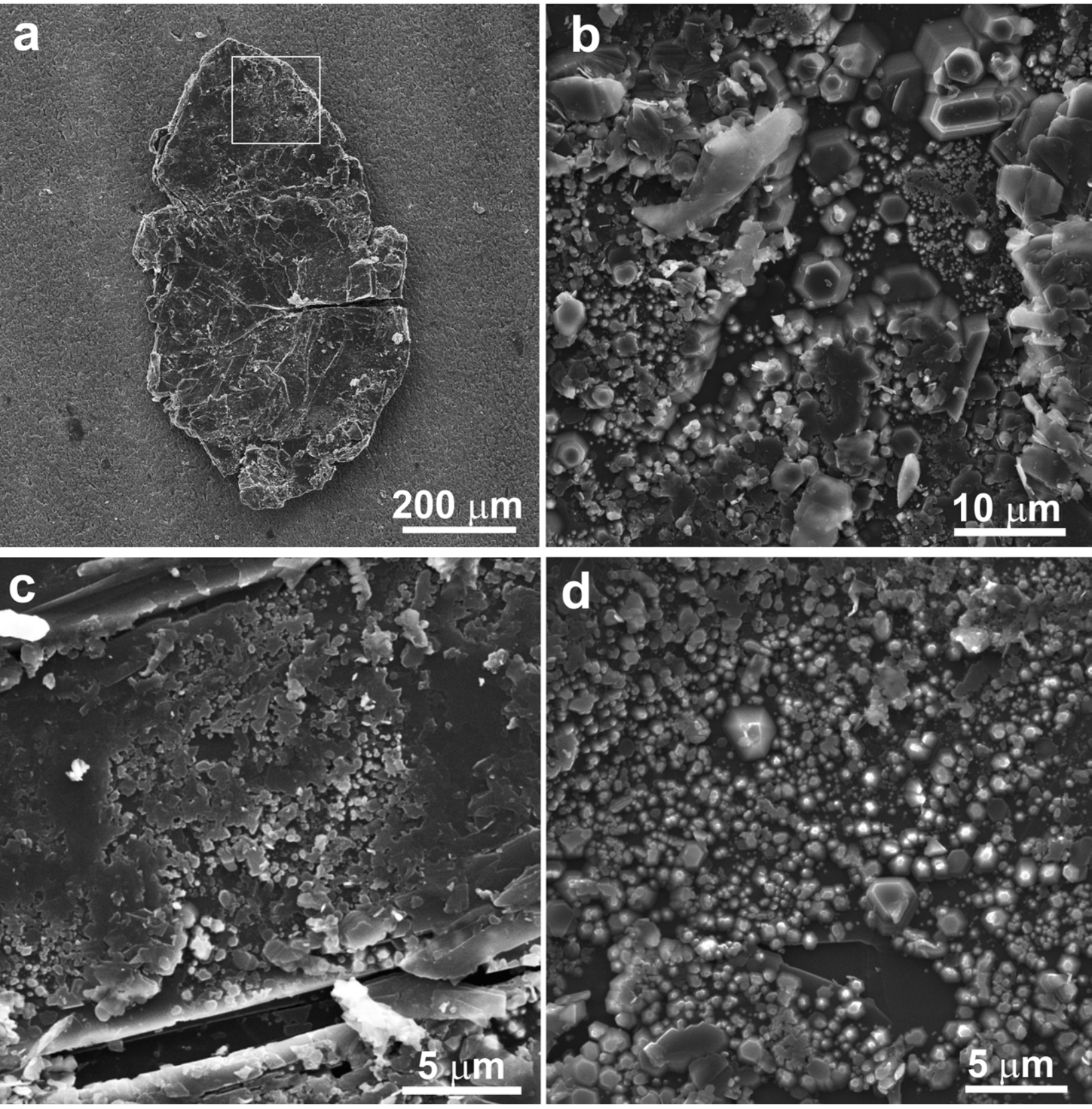

Figure 6

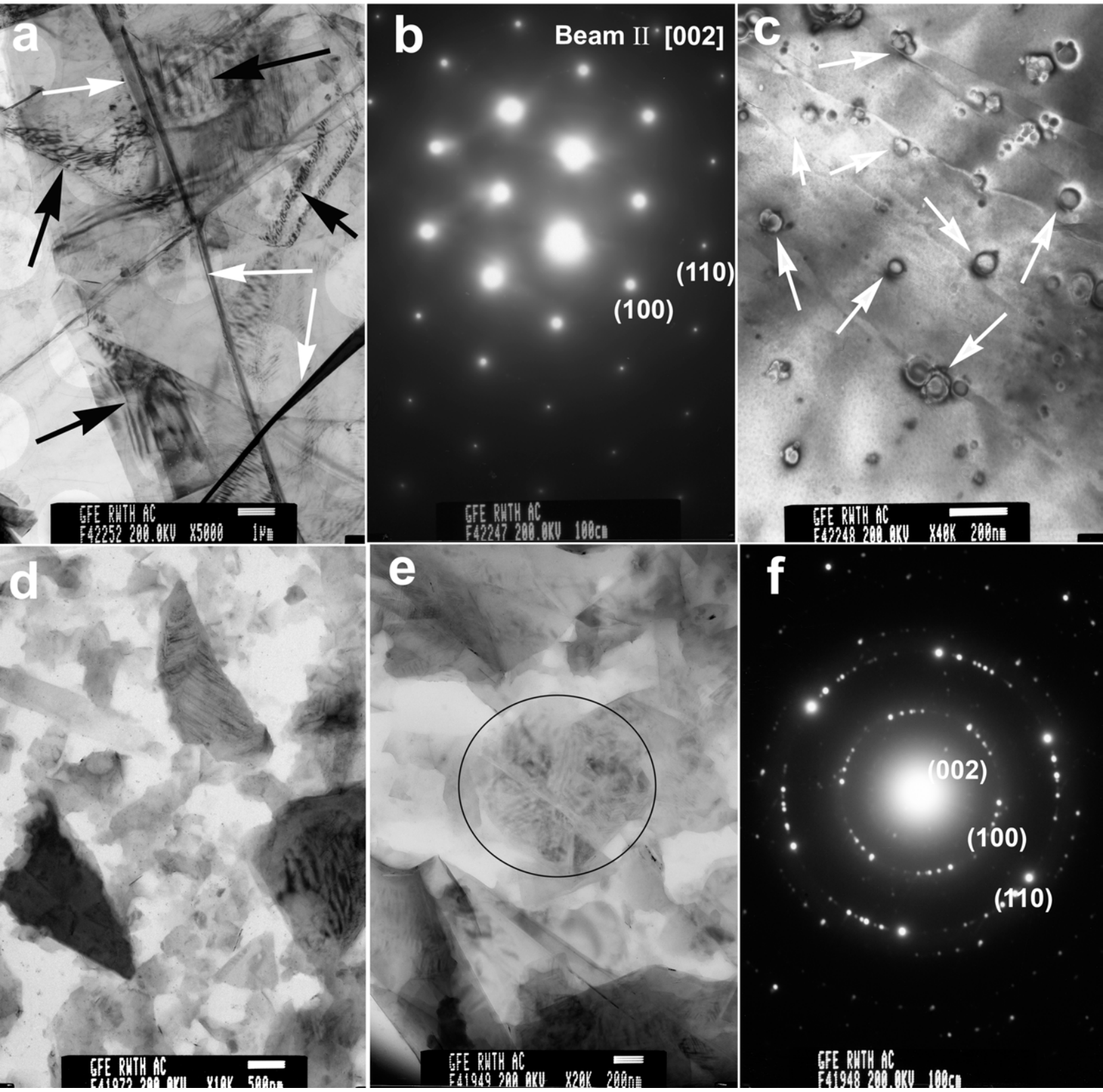
a
GFE RWTH AC
F42252 200.0KV X5000 1µm
b
Beam II [002]
(110)
(100)
GFE RWTH AC
F42247 200.0KV 100cm
c
GFE RWTH AC
F42248 200.0KV X40K 200nm
d
GFE RWTH AC
e
GFE RWTH AC
F41949 200.0KV X20K 200nm
f
(002)
(100)
(110)
GFE RWTH AC
F41948 200.0KV 100cm

Figure 7

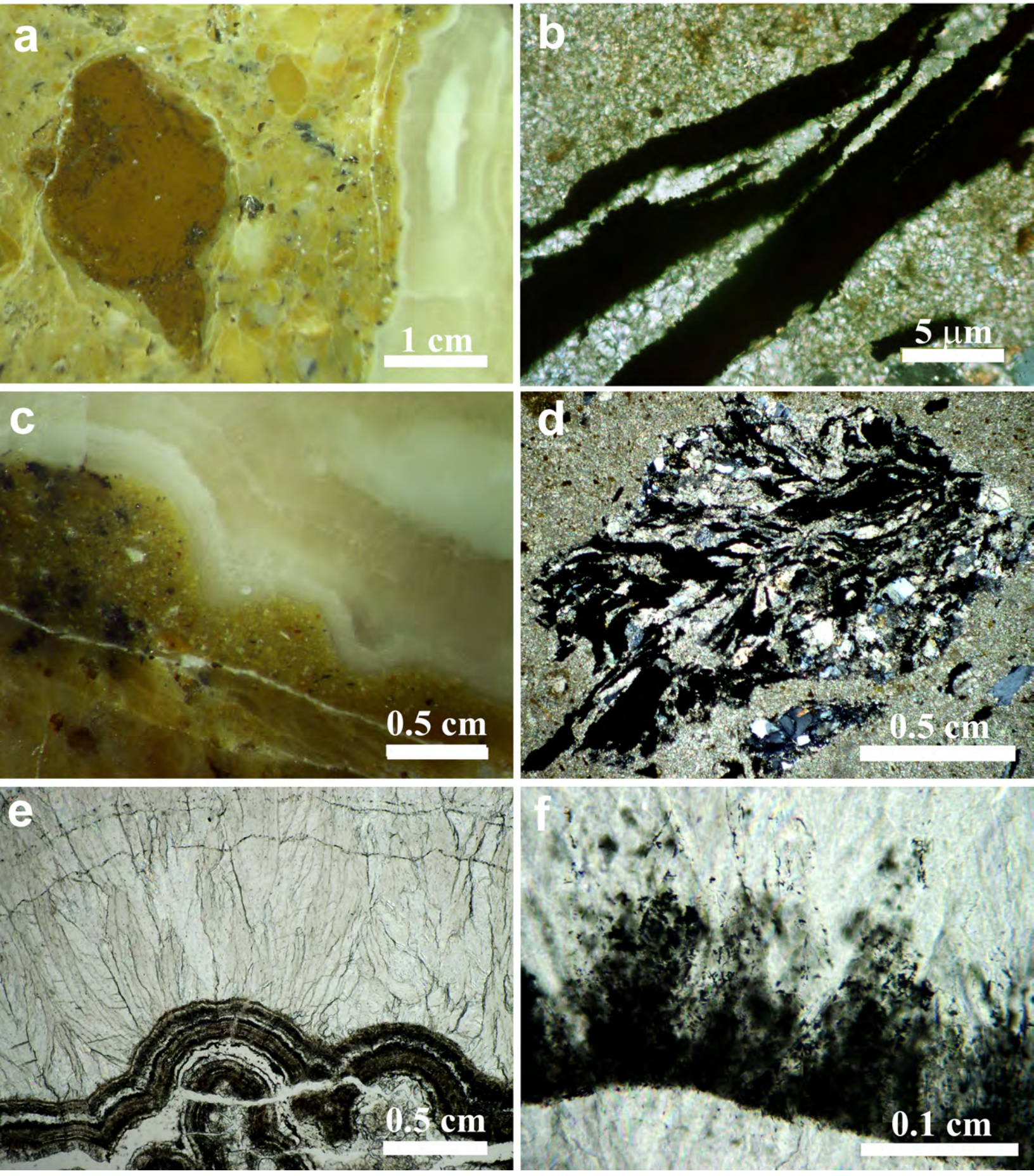

Figure 8

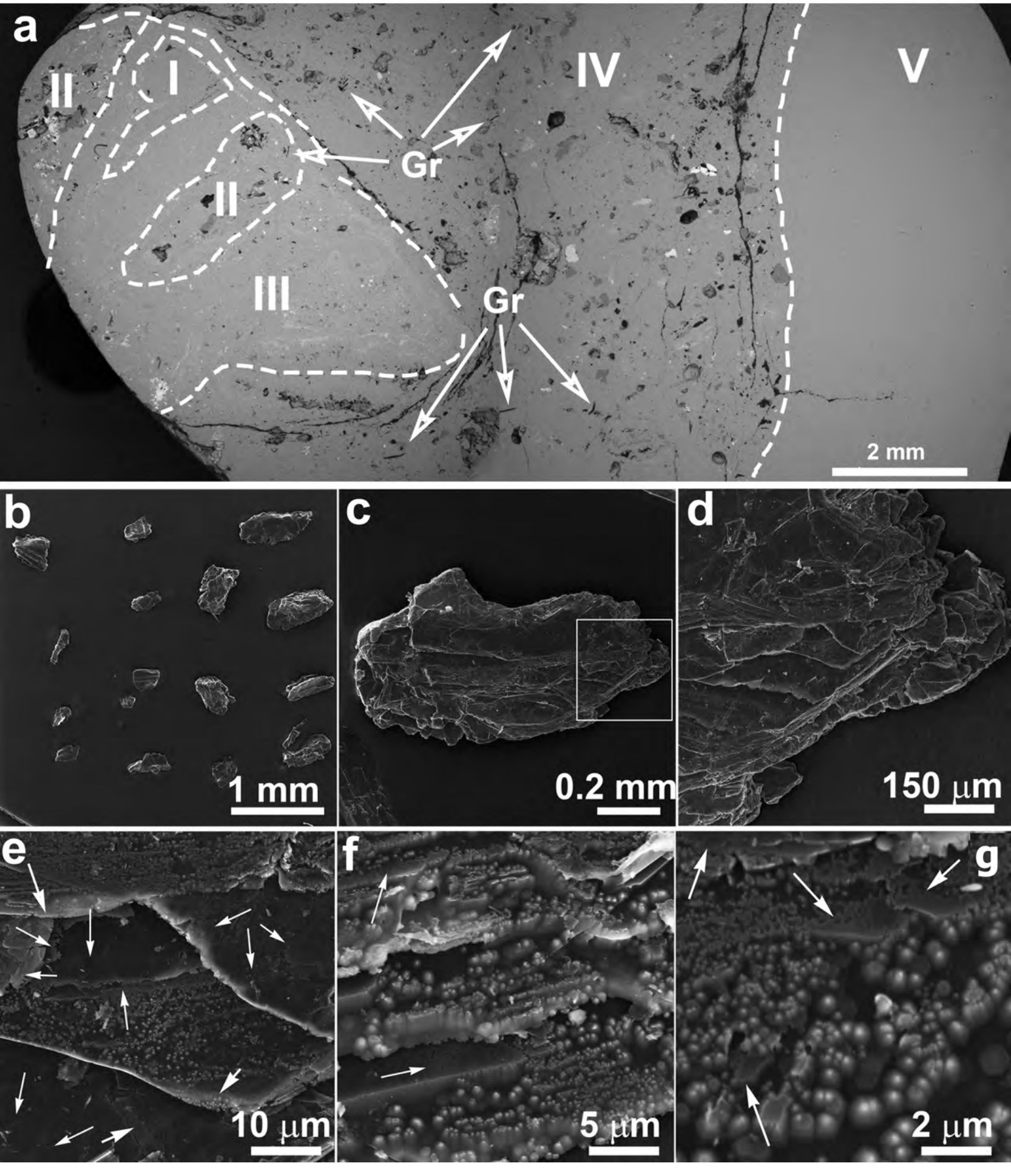

Figure 9

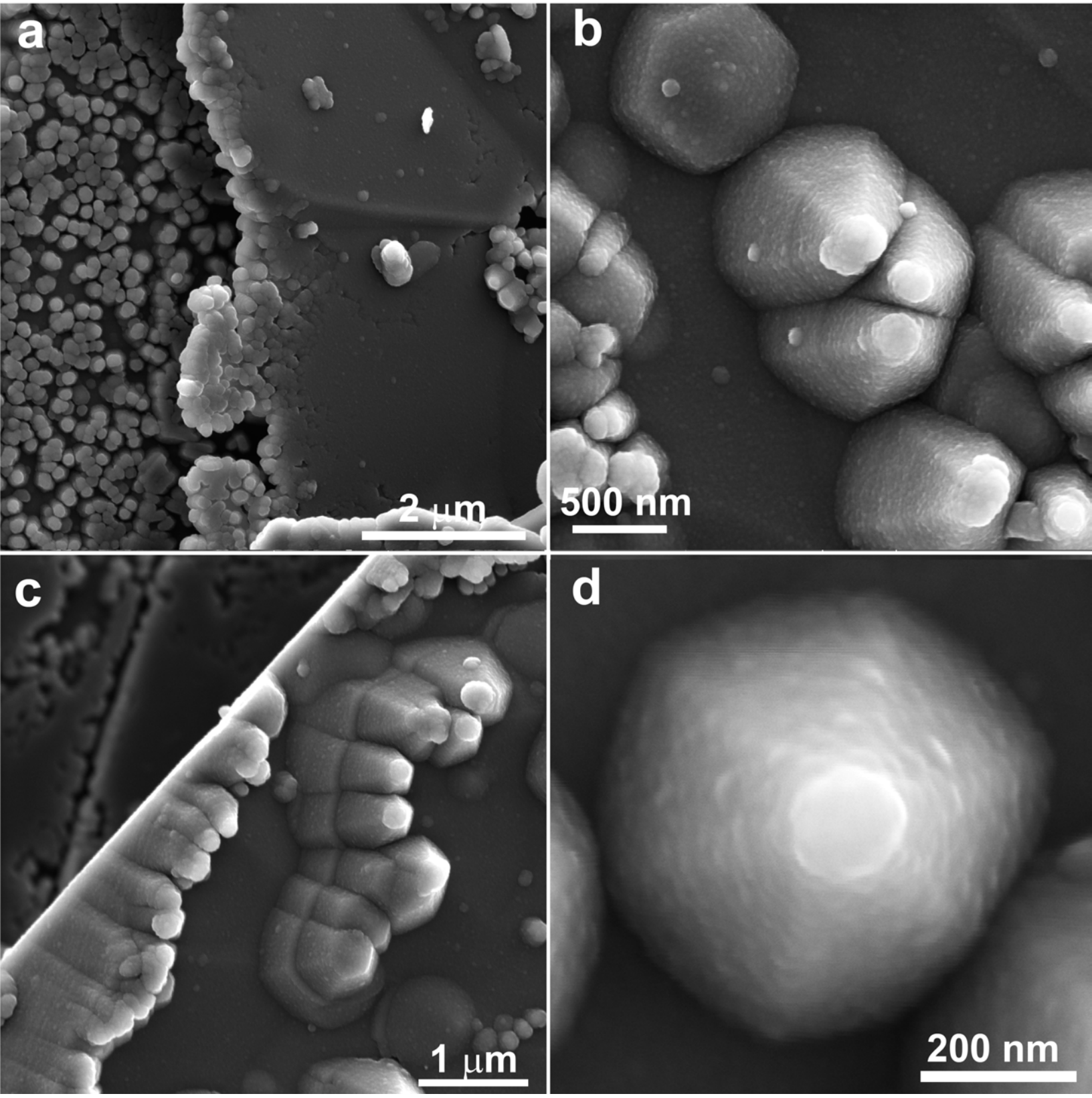

Figure 10

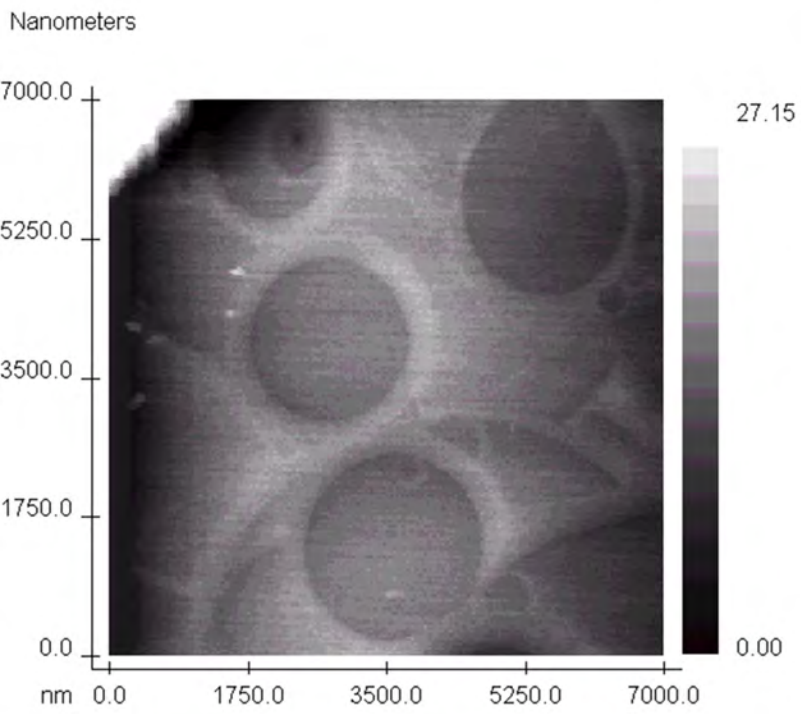
Nanometers
7000.0
5250.0
3500.0
1750.0
0.0
27.15
0.00
nm 0.0 1750.0 3500.0 5250.0 7000.0

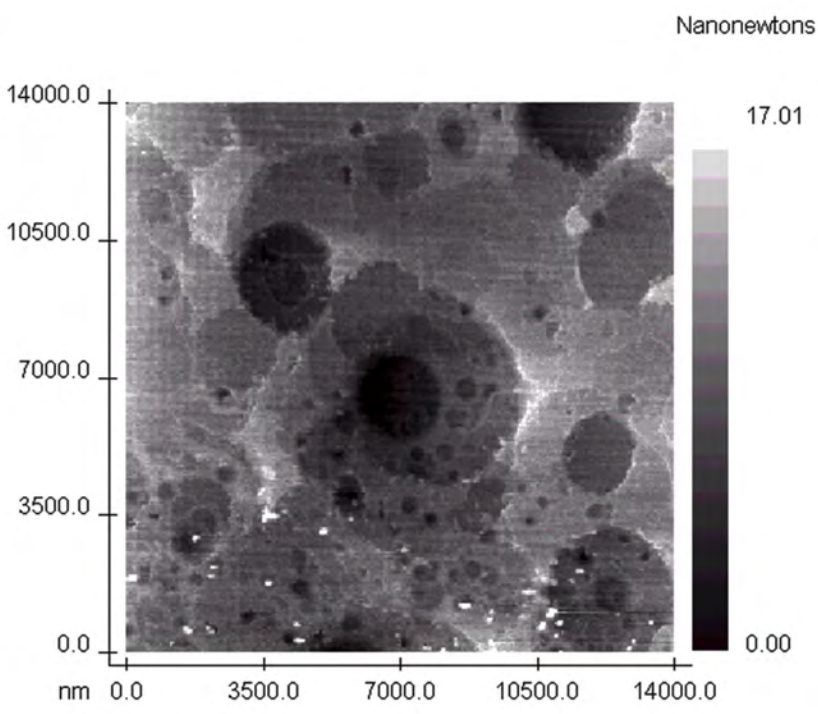
Nanonewtons
14000.0
10500.0
7000.0
3500.0
0.0
17.01
0.00
nm 0.0 3500.0 7000.0 10500.0 14000.0

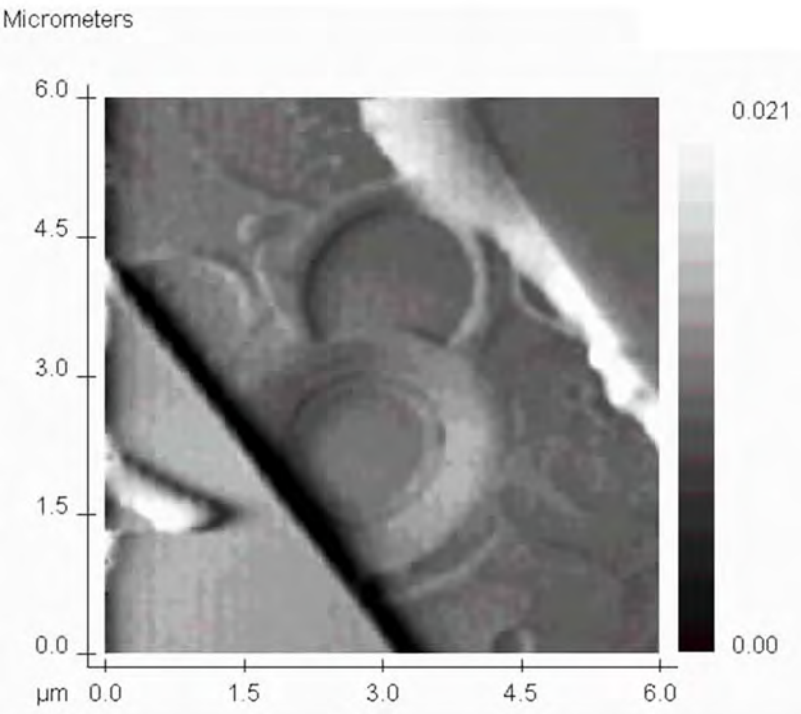
Micrometers
6.0
4.5
3.0
1.5
0.0
0.021
0.00
µm 0.0 1.5 3.0 4.5 6.0

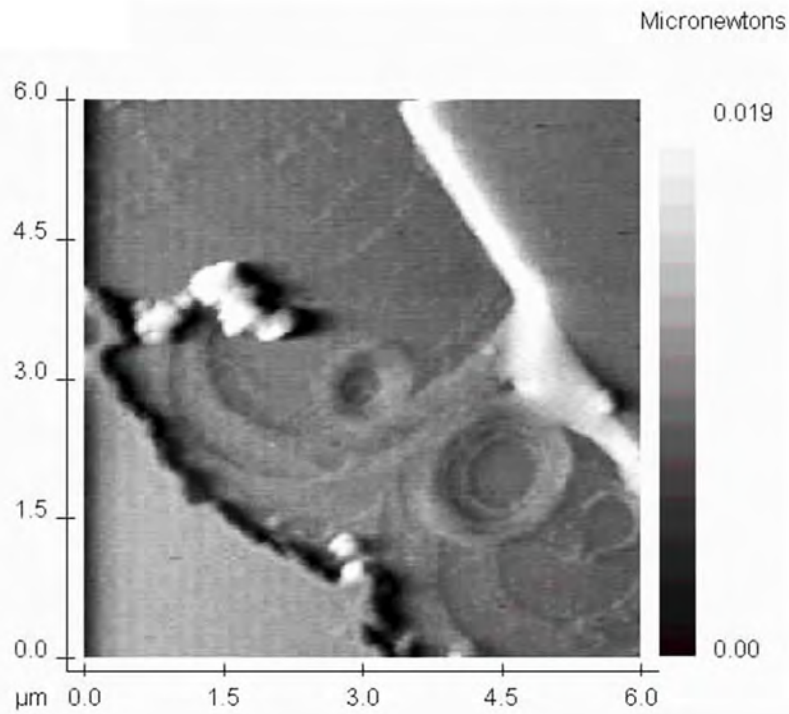
Micronewtons
6.0
4.5
3.0
1.5
0.0
0.019
0.00
µm 0.0 1.5 3.0 4.5 6.0

Figure 11

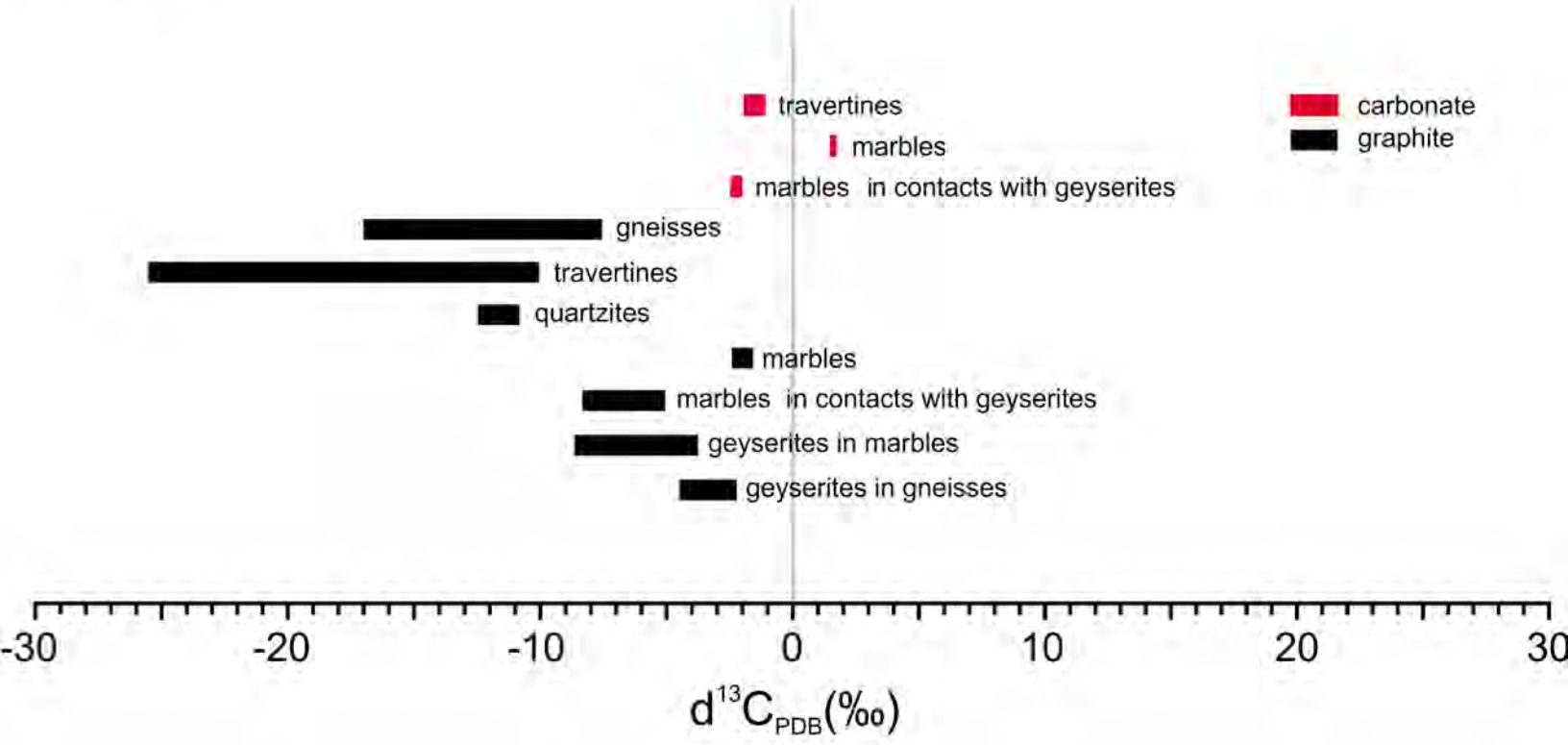
travertines
marbles
marbles in contacts with geyserites
gneisses
travertines
quartzites
marbles
marbles in contacts with geyserites
geyserites in marbles
geyserites in gneisses
carbonate
graphite
-30
-20
-10
0
10
20
30
d13CPDB(‰)

Figure 12

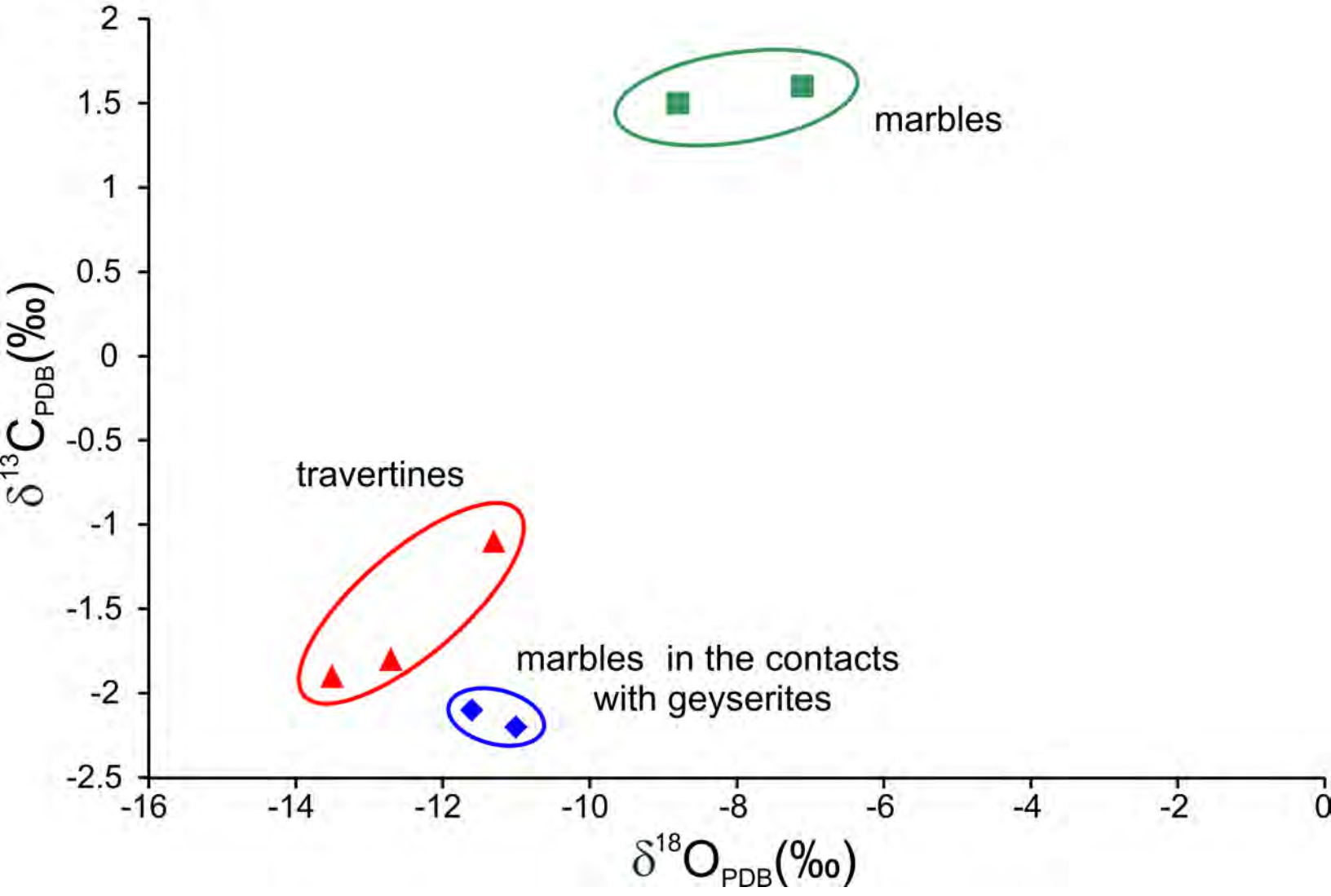
2
1.5
1
0.5
0
-0.5
-1
-1.5
-2
-2.5
-16
-14
-12
-10
-8
-6
-4
-2
0
δ13CPDB(‰)
δ18OPDB(‰)
marbles
travertines
marbles in the contacts
with geyserites

Figure 13

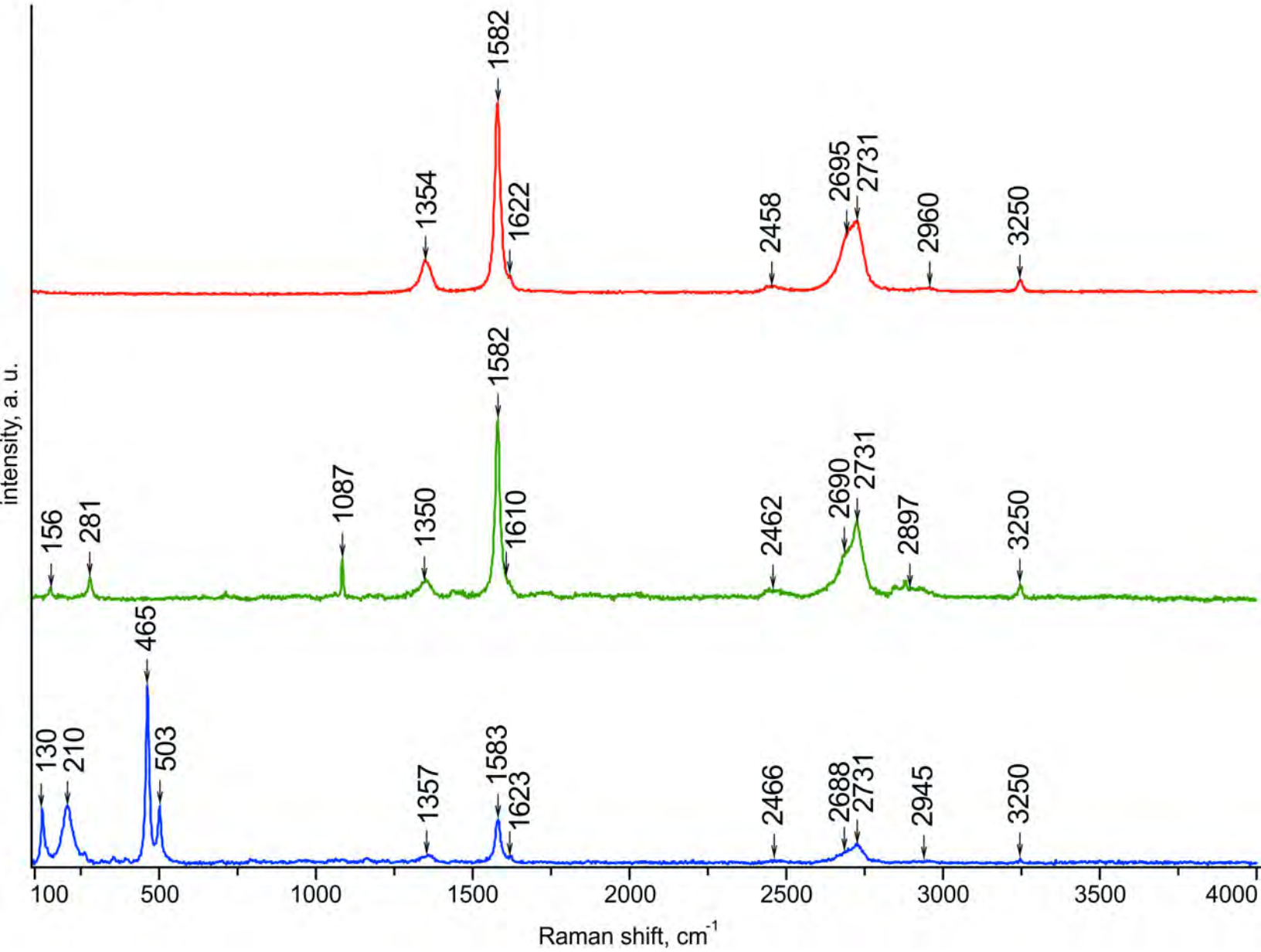
1582
1354
1622
2458
2695
2731
2960
3250
1582
156
281
1087
1350
1610
2462
2690
2731
2897
3250
465
130
210
503
1357
1583
1623
2466
2688
2731
2945
3250
intensity, a. u.
100
500
1000
1500
2000
2500
3000
3500
4000
Raman shift, cm-1

Figure 14

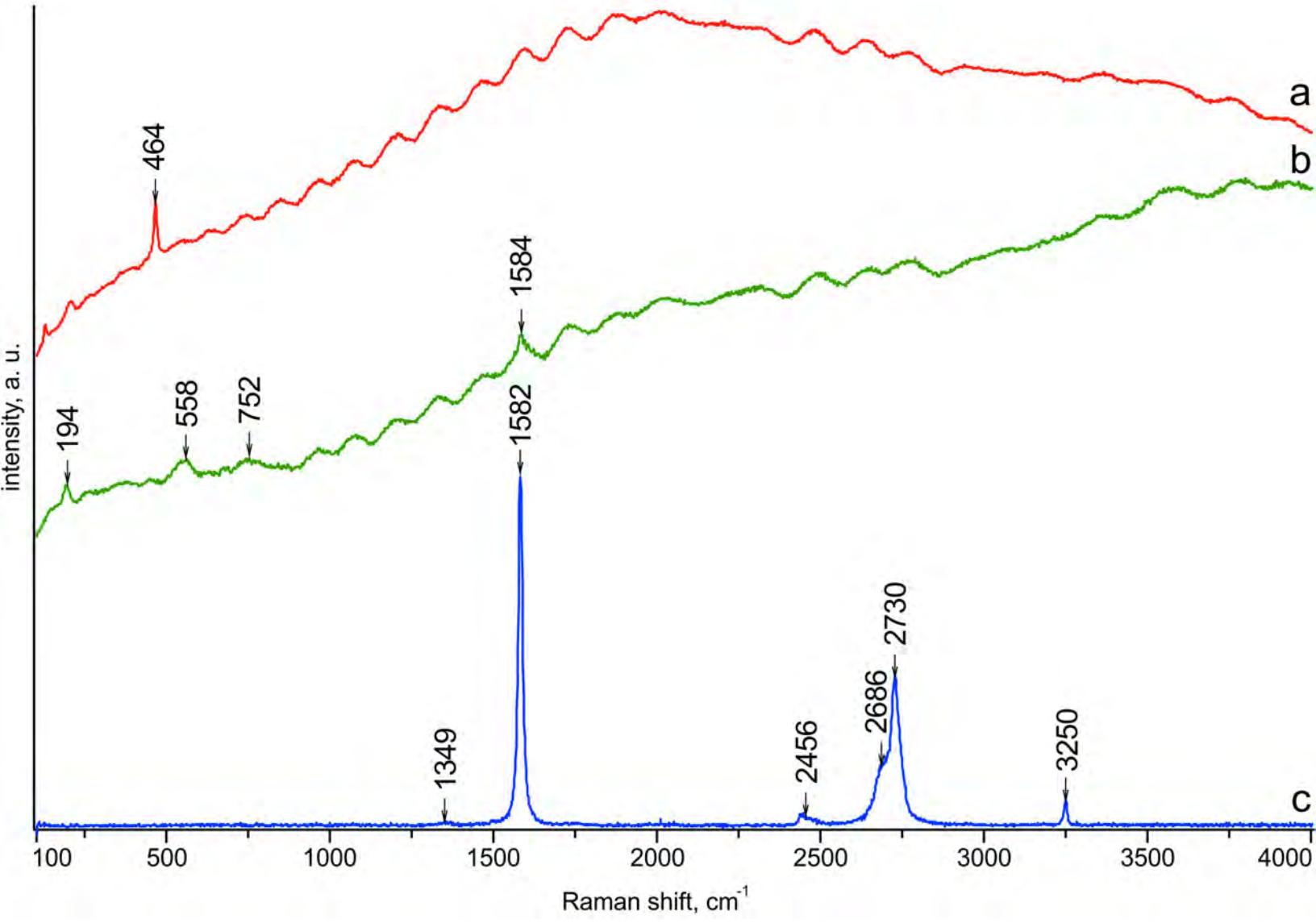
a
b
c
464
194
558
752
1584
1582
1349
2456
2686
2730
3250
intensity, a. u.
100
500
1000
1500
2000
2500
3000
3500
4000
Raman shift, cm-1